Computers and Geotechnics 163 (2023) 105751

Contents lists available at ScienceDirect

Computers and Geotechnics

journal homepage: www.elsevier.com/locate/compgeo

Catastrophic submarine landslides with non-shallow shear band propagation

Zhipeng Zhu [a], Dong Wang [a,b], Wangcheng Zhang [c,*]

[a] Key Laboratory of Marine Environment and Ecology, Ministry of Education, Ocean University of China, 266100 Qingdao, China
[b] Laboratory for Marine Geology, Qingdao National Laboratory for Marine Science and Technology, 266100 Qingdao, China
[c] Department of Engineering, Durham University, Lower Mount Joy, South Road, Durham DH1 3LE, UK

ARTICLE INFO

Keywords:
Submarine landslides
Shear band propagation
Clays
Strain softening
Finite element methods

ABSTRACT

Submarine landslides are a geohazard encountered frequently in both shallow and deep waters. Catastrophic landslides are often related to strain-softening and shear band propagation (SBP). Limit equilibrium methods cannot capture this mechanism. The existing SBP theoretical methods treat slope failure as a progressive process of SBP, however, based on the shallow SBP approximation which is only valid when the length of the initial shear band is much larger than its depth. In this paper, catastrophic propagation of a deep-seated shear band is investigated via finite element analyses to understand and quantify the SBP at different conditions. The shallow SBP approximation is tested in a parametric study in terms of the relative depth of shear band and soil properties. An empirical correction equation is introduced to account for non-shallow SBP by modifying the existing failure criteria. The empirical solution is compared well with the FE results and can be implemented to assess submarine slope stability. The influences of different strain-softening relationships and inertia effects are discussed as well. As an example, the historical Storegga Slide offshore Norway is revisited, and the critical condition for its catastrophic failure is quantified using the proposed criterion.

1. Introduction

Submarine landslides frequently occur in both shallow and deep waters, threatening the safety of on-bottom infrastructures such as subsea production systems, pipelines, and cables (Hill et al., 2015; Lin et al., 2010). Compared with their subaerial counterparts, submarine landslides are typically characterized by lower slope angles, much larger sliding mass volumes, and longer runout distances (Masson et al., 2006; Akinci and Sawyer, 2016). A notable example is the second Storegga Slide, which occurred about 8200 years ago on the Norwegian continental slope with an inclination $< 2^{\circ}$, involving 3000 km^3 of debris that ran out for over 800 km (Kvalstad et al., 2005a; Vanneste et al., 2014). To evaluate the potential hazards of submarine landslides, it is crucial to comprehend their triggering mechanisms and to accordingly quantify slope failure.

The limit equilibrium method, which assumes that the soils along the potential slip surface reach the failure state simultaneously, is arguably the most popular approach used in slope stability analyses (Duncan, 1996). This assumption is plausible for relatively steep slopes (Kaya et al., 2016). However, for submarine slides with inclinations $< 10^{\circ}$, a more realistic mechanism is that the failure is initiated over a limited length of the weak layer, forming an initial shear band which then propagates into the adjacent intact soils until a catastrophic failure occurs (Micallef et al., 2007). The shear band propagation (SBP) is highly dependent on the strain-softening behavior of marine sediments, where the intact soil is remolded due to shearing (L'Heureux et al., 2012; Leynaud et al., 2017), causing the spontaneous growth of shear band under existing gravity forces. A number of theoretical (Locat et al., 2011; Palmer and Rice, 1973; Quinn et al., 2011) and numerical (Chen et al., 2021; Dey et al., 2015; Quinn et al., 2012; Troncone et al., 2022, 2023) analyses have been conducted to account for the progressive failures of gentle slopes. Compared to the limit equilibrium method, these methods establish a more conservative and appropriate basis for slope stability assessments.

The SBPs for a particular type of initiation history have been investigated in Dey et al. (2016), Germanovich et al. (2016) and Stoecklin et al. (2017) among others, where an initial fully softened zone with length l_0, termed pre-softened zone, is wished in place in an elasto-plastic weak layer, as illustrated in Fig. 1. This initiation scenario can be caused by factors such as earthquakes (Liu et al., 2022; Strasser et al., 2007), salt diapirism (Kovacevic et al., 2012), toe erosion (Wang et al.,

* Corresponding author.
E-mail addresses: zhuzhipeng6219@stu.ouc.edu.cn (Z. Zhu), dongwang@ouc.edu.cn (D. Wang), wangcheng.zhang@durham.ac.uk (W. Zhang).

https://doi.org/10.1016/j.compgeo.2023.105751
Received 30 May 2023; Received in revised form 7 August 2023; Accepted 16 August 2023
Available online 25 August 2023

Nomenclature

a, b	parameters related to the failure criteria in terms of length of pre-softened zone
E, E_{ps}, ν	uniaxial and plane strain Young's modulus, the Poisson's ratio.
G_s	shear stiffness of shear band
g, g_{acc}	gravity acceleration, accumulated gravity acceleration in FE analyses
h, s	thickness of sliding layer and weak layer
k	strength ratio of shear band
l, l_0, ω, L	length of shear band, pre-softened and process zones, and slope model
l_u	characteristic length of shear band
$\hat{l}_0, \hat{h}$	length and thickness normalized by l_u
O, x, y	origin, horizontal and vertical coordinate
S_t	soil sensitivity
t	time
z	depth of soils
u_x, u_{x0}	downslope displacement of sliding layer and u_x at origin
α	correction factor
β	parameters related to process zone length
γ	shear strain
Δ	net changes of variables
δ	shear displacement of shear band, superscripted by 'e' and 'p' for elastic and plastic component
δ_r^p	value of δ^p at residual state
δ_{95}^p	value of δ^p to achieve 95% reduction in shear strength
θ	slope angle
Λ	characteristic depth parameter
ρ, ρ'	saturated and submerged density
σ_{v0}'	initial vertical effective stress
σ_x	normal stress of sliding layer
$\overline{\sigma}_x, \overline{u}_x$	average value of σ_x, u_x along the depth
τ, τ_g	mobilized and gravitational shear stress of shear band
$\tau_{g,cri}$	critical value of τ_g to trigger catastrophic SBP
$\tau_{g,cri}^{ana}$	value of $\tau_{g,cri}$ obtained from analytical SBP failure criteria
τ_0	shear strength of initial fully softened zone
τ_p, τ_r, τ_{ave}	peak and residual value of shear strength of shear band, average peak strength of sliding layer
$\hat{\tau}_g$, $\hat{\tau}_0$, $\hat{\tau}_{g,cri}$	value of τ_g, τ_0 and $\tau_{g,cri}$ normalized by τ_p
ψ	cut angle at the front and rear faces

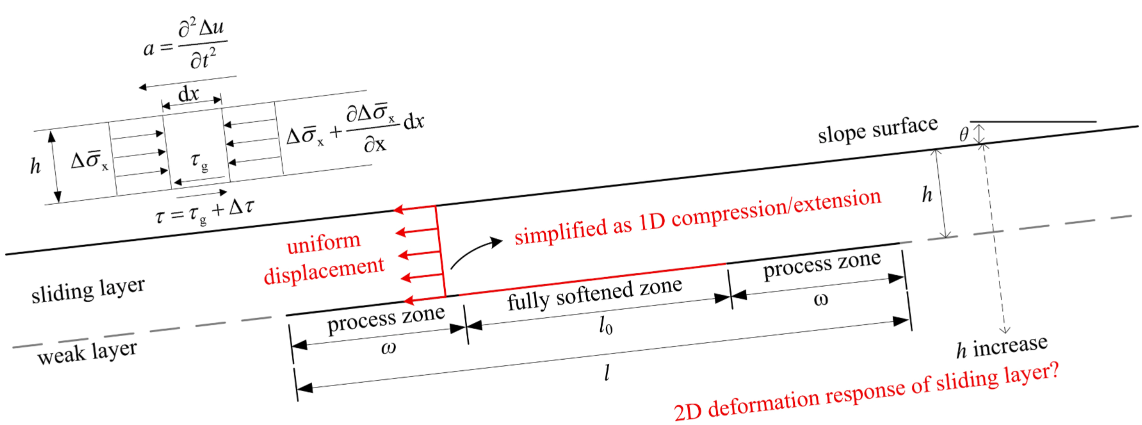

Fig. 1. Shallow shear band propagations caused by an initial fully softened zone with forces acting on a slice presented on top left.

2021), hydrate decomposition (Sultan et al., 2004) and fluid migration (Elger et al., 2018; Lafuerza et al., 2012). As the driving force (e.g. by self-weight or seismic load) exceeds the resistance inside the pre-softened zone, the shear band propagates into the process zone with length ω. Depending on the magnitude of the driving force, the propagation becomes limited (progressive SBP) or evolved into a landslide (catastrophic SBP). A number of analytical failure criteria have thus been developed to account for quasi-static conditions (Puzrin et al., 2004, Zhang et al., 2015), inertia effects (Germanovich et al., 2016; Zhang et al., 2016), curvilinear slopes (Puzrin et al., 2015) and three-dimensional slopes (Zhang and Puzrin 2022). However, these SBP methods are valid only when the thickness of the sliding layer h is remarkably smaller than the total length of the initial shear band $l = l_0 + 2\omega$ (see Fig. 1), i.e. $h \ll l$. Based on the shallow SBP approximation, the response of sliding layer is simplified as a one-dimensional problem, where the displacement along the depth is assumed to be uniform, guaranteeing that the solutions of most existing analytical criteria are available. However, before applying these criteria, one should check the consistency between the results obtained and the shallow SBP approximation.

For the submarine landslide with a deep slip surface, such as the Storegga Slide with $h > 200$ m, the assumption of shallow SBP may not be satisfied. In non-shallow cases, the actual displacement distributions within the sliding layer may differ from the shallow approximation, leading to a divergence between the physical and existing analytical failure criteria. Therefore, further investigation is required to interpret the failure criteria with a non-shallow slip surface, thereby enabling more reliable slope stability assessments.

Parallel to the above studies with an elasto-plastic slip surface, in a similar vein, the growth of slip-weakening rupture has been investigated within the framework of linear elastic fracture mechanics. It has been found that the concentration of shear stress or elevated pore pressure on fault can trigger rupture propagation and consequently a landslide (Uenishi and Rice, 2003; Garagash and Germanovich, 2012). The effects of the aspect ratio of crack length and depth were explored in a similar fashion in Bažant et al. (2003) and Viesca and Rice (2012). Although failure criteria with a non-shallow slip surface were established for linear elastic materials, such as rocks, dry snow or hard clays, these studies may not be suitable for sands or normally consolidated clays which exhibit intrinsically non-elastic behavior and are common in marine sediments.

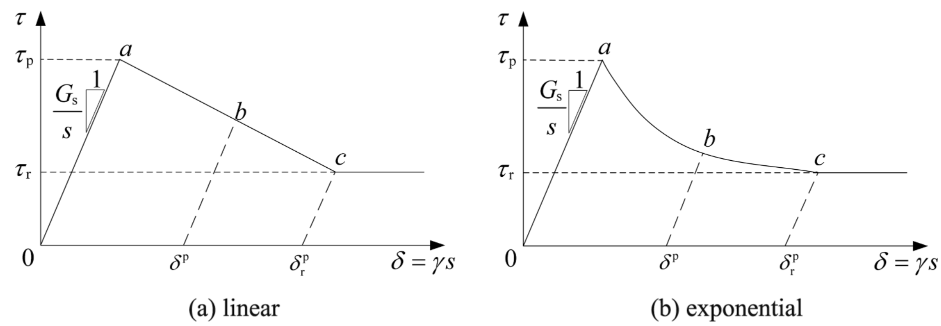

Fig. 2. Strain-softening relationship of soil in the shear band.

This paper aims to interpret the SBPs under non-shallow conditions, where the shear band is treated as an elasto-plastic material. The evolutions within the shear band and the sliding layer, induced by an initial pre-softened zone, are investigated using the finite element (FE) method. The FE results under static conditions with the linear strain-softening response of shear band are compared with the existing analytical solutions, followed by the interpretation of the failure mechanic and criterion under non-shallow conditions. An empirical but simple correction equation is proposed to predict the slope stability of non-shallow cases by modifying the existing analytical SBP criterion. Then, an example study is provided to illustrate the application of the proposed criterion. Finally, the effects of different strain-softening behavior of the shear band and the inertia of the sliding layer are investigated, respectively.

2. Methodology

2.1. Problem definition

The problem of slope instability with SBP is idealized in Fig. 1, where a pre-softened zone of length l_0 is formed within a weak layer of an infinite slope. The slope is inclined at an angle θ. The sliding layer, with thickness h, above the weak layer is simplified as linear elastic material since no failure is expected prior to the catastrophic SBP. The weak layer, with thickness s, is assumed to be elasto-plastic with a linear or exponential strain-softening response. A stiff base is set beneath the weak layer. Due to external triggering, the shear strength of the pre-softened zone is fully reduced to τ_0, lower than the shear stress by gravity τ_g, forming the initial driving force. A process zone of length ω is thus mobilized gradually at each tip of the pre-softened zone, where the shear strengths are decreased from the peak value τ_p to the residual τ_r due to strain-softening. Note that τ_0 in the pre-softened zone may differ from τ_r in the process zone depending on the weakening mechanism. Outside the pre-softened and process zones, the sediments within the weak layer remain intact and undergo elastic shearing.

The shear stress within the process zone is limited by current shear strength, which is assumed to be compressed linearly to the peak, followed by linear or exponential degradation, as depicted in Fig. 2. In the elastic region, the shear stress τ is given by

$$\tau = \frac{G_s}{s}\delta^e \tag{1}$$

where G_s is the shear stiffness of shear band, δ^e the elastic component of shear displacement δ. The shear displacement δ is related to the thickness of weak layer s and the shear strain γ by $\delta = \gamma s$. The response for linear degradation is given by

$$\tau = \max\left[\tau_p + (\tau_r - \tau_p)\frac{\delta^p}{\delta^p_r}, \tau_r\right] \tag{2}$$

where δ^p_r the value of plastic shear displacement δ^p at residual. For exponential strength degradation, the shear stress is given by

$$\tau = \max\left[\tau_r + (\tau_p - \tau_r)e^{-3\delta^p/\delta^p_{95}}, \tau_r\right] \tag{3}$$

where δ^p_{95} is the value of δ^p to achieve 95% reduction in shear strength. The peak strength of the weak layer τ_p is expressed as

$$\tau_p = k\sigma'_{v0} \tag{4}$$

where k is the undrained shear strength ratio, $\sigma'_{v0} = \rho' gh$ the initial effective vertical stress on the shear band, ρ' the submerged soil density and g = 9.8 m/s^2 the gravitational acceleration. The residual shear strength is given by

$$\tau_r = \tau_p / S_t \tag{5}$$

where S_t is soil sensitivity.

2.2. Background of analytical SBP analyses

Three approaches, linear elastic fracture mechanics, energy balance and process zone approaches, have been developed to derive analytical failure criteria based on the shallow SBP approximation. The former two approaches assume that the length of process zone ω is negligible, i.e. $\omega \ll h \ll l$, while the latter assumes that $h \ll \omega < l$. The framework of the process zone approach is introduced below, as the significance of process zone has been approved (Zhang et al. 2015).

For convenience, the 'net' values of variables, represented by the symbol 'Δ', are considered in the analytical analyses with respect to the counterpart in the slope without any initial failure. The derivations of static and dynamic SBP criteria for this problem are similar, except that the latter accounts for the inertial effect. The static SBP criteria are applicable when the pre-softened zone is gradually formed with insignificant kinetic energy, whereas the dynamic SBP criteria take into account the kinetic energy resulting from the rapid formation of the pre-softened zone.

According to the Newton's second law, the equilibrium of an elementary sliding layer is given by

$$h\frac{\partial \Delta\overline{\sigma}_x}{\partial x} - \Delta\tau = \rho h\frac{\partial^2 \Delta\overline{u}_x}{\partial t^2} \tag{6}$$

where $\Delta\overline{\sigma}_x$ is the net average normal stress of the sliding layer; $\Delta\tau$ the net mobilized shear stress of the shear band; $\rho h\partial^2\Delta\overline{u}_x/\partial t^2$ the inertia term, which is ignored under the static conditions; ρ the saturated soil density; $\Delta\overline{u}_x$ net average normal displacement of the sliding layer; and t the time. For a shallow SBP with $h \ll l$, the sliding layer response can be treated as a one-dimensional compression/extension problem, and the $\Delta\overline{u}_x$ of sliding layer is assumed to be identical to the shear displacement $\Delta\delta$ of shear band, so that $\Delta\overline{\sigma}_x$ can be given by

$$\Delta\overline{\sigma}_x = E_{ps}\frac{\partial \Delta\overline{u}_x}{\partial x} = E_{ps}\frac{\partial \Delta\delta}{\partial x} \tag{7}$$

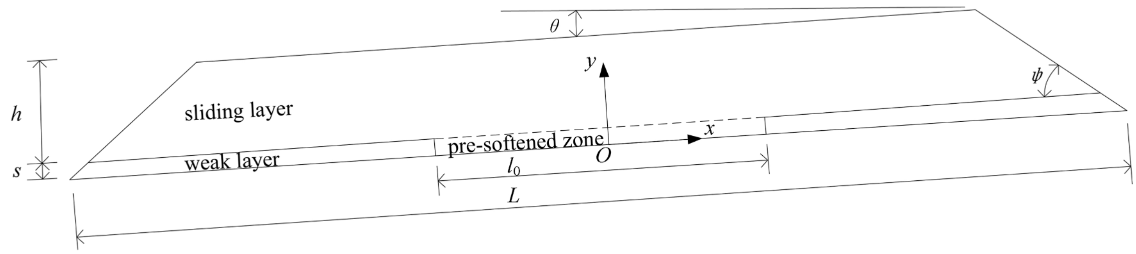

Fig. 3. Slope model with the existence of a pre-softened zone in the FE analyses.

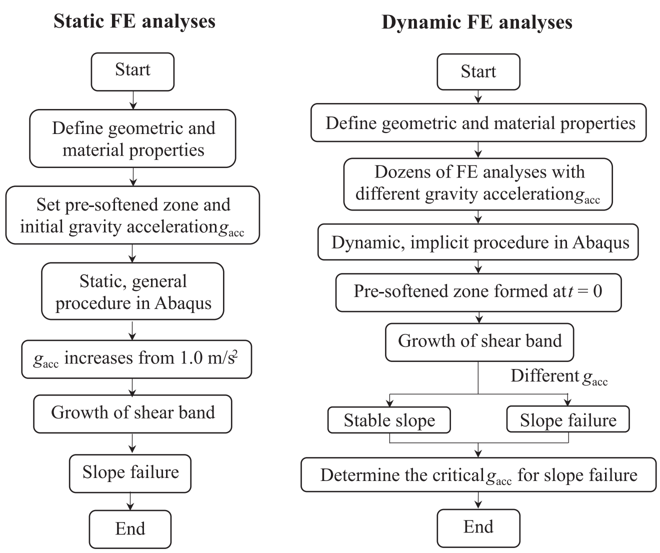

Fig. 4. Flow chart of the static and dynamic FE analyses.

where $E_{ps} = E/(1-\nu^2)$ is the Young's modulus under plane strain conditions, E the uniaxial Young's modulus and ν the Poisson's ratio.

By combining Eqs. (1)–(7), the distributions of $\Delta\tau$ and $\Delta\delta$ within the shear band can be solved. Therefore, the failure criteria can be deduced analytically based on the stress distribution within the shear band at the critical condition. For static conditions, the maximum resistance force is reached when the shear strength at the interface between the pre-softened and process zones is softened to τ_g. With any increase of driven force, the process zone would be further softened and generate additional driven force, causing the catastrophic SBP.

For linear strain-softening soils in the shear band, the static failure criterion in terms of the length of pre-softened zone l_0 is given by (Zhang et al., 2015)

$$l_0 > l_{cri} = \frac{2l_u(\tau_p - \tau_g)}{\tau_g - \tau_0} \tag{8}$$

$$l_u = \sqrt{E_{ps} h \delta_r^p / (\tau_p - \tau_r)} \tag{9}$$

where l_u is the characteristic length of the shear band for linear degradation. For a given l_0, rewriting Eq. (8), the gravitational shear stress τ_g at the critical condition for catastrophic SBP is given by

$$\tau_{g,cri} = \frac{l_0 \tau_0 + 2 l_u \tau_p}{l_0 + 2 l_u} \tag{10}$$

The length of process zone ω is given by

$$\omega = l_u \beta \arcsin(\beta) \tag{11}$$

$$\beta = \sqrt{1 - \frac{(\tau_p - \tau_r)s}{G_s \delta_r^p}} \tag{12}$$

The static failure criteria with exponential strength degradation response and the dynamic failure criteria are not detailed here, which can be found in Zhang et al. (2015, 2016).

As highlighted above, the analytical expressions of failure criteria were based on the approximation of shallow SBP, i.e. Eq. (7). This approximation becomes gradually violated with the increase of relative depth h/l. Therefore, the FE analyses are conducted below to investigate the slopes with non-shallow SBPs.

2.3. Finite element model

Fig. 3 displays the planar slope model used in FE analyses. The slope is shaped as a long embankment with an overall length of L, to mimic part of an infinite slope. The front and rear faces of the model are cut at an angle of ψ to ensure that the failure occurs in the middle rather than at the sides of the weak layer. The sliding layer is set as a linear elastic material, while the stiff base is simplified as a rigid boundary. The stress–strain relationship in the weak layer is depicted in Fig. 2, identical to those used in the theoretical analyses. Since the strain-softening behavior of the weak layer is essentially governed by shear displacement $\delta = \gamma s$ rather than shear strain γ, the mesh dependency is avoided in the FE analyses.

The FE analyses with the implicit integration scheme are conducted using the commercial package Abaqus (Dassault Systèmes, 2014). The soil in the shear band undergoes limited but not extremely large deformations prior to the catastrophic failure, and therefore, the simulations are based on finite strain formulations. The slope is discretized with four-node quadrilateral elements with full integration. A convergence analysis on the mesh size and layers of weak layer was conducted in trial calculations. It is found that the shear band only covers one layer of elements, and mesh sensitivity relevant to strain-softening can be avoided by using the stress-displacement response as discussed above. Therefore, a weak layer with a single layer of elements and element size $s = 0.5$ m was used in the study. A finer mesh is set above the weak layer with the minimum element size equal to the thickness of weak layer s. The overall length of the slope L is set to be >80 h, which ensures that the slope toes are sufficiently far from the central.

The SBP studied here is caused by gravity loading. Flow charts for the static and dynamic FE analyses are shown in Fig. 4. For static FE analyses, the gravity load of the slope is artificially increased to trigger the catastrophic SBP. The accumulated gravity acceleration of slope g_{acc} is ramped up from 1.0 m/s^2 with an increment of $\Delta g_{acc} = 0.01$ m/s^2. Note that under certain soil properties and pre-softened zone length, the critical acceleration for catastrophic SBP g_{acc} may fall below the gravitational acceleration 9.8 m/s^2, which indicates that the slope failure is deemed happen in reality. Otherwise, the slope stability factor can be assessed to ascertain the safety margin. The accumulated gravitational shear stress is calculated as

$$\tau_g = \rho' g_{acc} h \sin\theta \tag{13}$$

The strain softening is expected to develop at each end of the pre-softened zone by gradually increasing the gravity load. The critical condition for catastrophic SBP is identified as the soil strength at the interface between the pre-softened and process zones is softened to the

Table 1
Parameters for numerical analyses.

Parameter	Base value	Parametric studies	Unit
Overall embankment length, L	80h	–	m
Thickness of shear band, s	0.5	–	m
Slope angle, θ	5	–	degrees
End-slope angle, ψ	15	–	degrees
Poisson's ratio, ν	0.495	–	
Rigidity index in softening layer, G_s/τ_p	166.7	–	
Saturated (submerged) density of soil, $\rho(\rho')$	1700 (700)	–	kg/m^3
Thickness of sliding material, h	50	10, 30, 50, 100 and 200	m
Normalized length of pre-softened zone, l_0/h	1	0.33, 0.5, 1, 2, 4, 6, 8, 10, 15, 20 and 40	
Strength ratio of pre-softened zone, τ_0/τ_p	0.33	0.1, 0.2, 0.33, 0.5 and 0.67	
Average Young's modulus ratio for sliding layer, E/τ_p	250	150, 200, 250, 300 and 400	
Undrained shear strength ratio, k	0.2	0.15, 0.2, 0.25, 0.3 and 0.35	
Sensitivity, S_t	3	1.5, 2, 3, 5 and 10	
Plastic shear displacement to residual,δ_r^p	0.2	0.05, 0.1, 0.2, 0.4 and 0.8	m

current τ_g, after which the slope failure occurs soon. For dynamic FE analyses, the pre-softened zone is set to form instantaneously, resulting in SBP under a given τ_g. For each case, dozens of FE simulations with various values of τ_g are conducted to determine the critical τ_g for catastrophic SBP. It is worth noting again that the strength parameters are determined against the self-weight of soil with $g = 9.8$ m/s^2 despite the artificial change of gravity loading.

The parameters used in the numerical studies, as listed in Table 1, were determined based on the soil properties reported in Kvalstad et al. (2005b) and Randolph et al. (2005). For marine clays, the typical range of soil sensitive S_t is 2 to 5, although can be as high as 10 (L'Heureux et al., 2012). The plastic shear displacement leading to the residual state of soils typically ranges from 0.05 to 0.8 m (Skempton 1985; Dey et al., 2016). The base values of parameters are applied unless otherwise stated.

3. Numerical results

The critical condition for catastrophic SBPs under the static condition is explored numerically with a linear strain-softening response of the shear band. For simplicity, only the response on the left side of the slope is presented, as the slope is symmetric to the centre of the pre-softened zone in terms of the shape. Displacements are defined to be positive in the downslope direction.

3.1. Examination of the shallow SBP approximation

As mentioned earlier, the shallow SBP approximation ($h \ll l$) assumes that the net average normal displacement $\Delta\overline{u}_x$ within the sliding layer is identical to the net shear displacement across the shear band $\Delta\delta$, which is key to deriving the analytical failure criteria. The distribution of net normal displacements Δu_x at the occurrence of the catastrophic SBP is investigated to examine this assumption. Since the length of process zone ω is unknown at the commencement of calculation, h/l_0 is ranged between a typical shallow condition ($h/l_0 = 0.05$) and a relatively deep one ($h/l_0 = 1$) despite h being fixed at 50 m.

The numerical net displacements Δu_x are normalized by the net normal displacement at the middle of the pre-softened zone Δu_{x0}. The value of Δu_x at the bottom of the sliding layer is consistent with the shear displacement $\Delta\delta$ at the shear band. As shown in Fig. 5a, for the weak layer buried shallowly, Δu_x is almost uniform along the depth, satisfying the assumption of the shallow SBP, although Δu_x above the process zone and elastic zone varies slightly along the depth. When h/l_0 is increased to 0.25, values of Δu_x at the top and bottom of the sliding layer are remarkably different from each other. At $h/l_0 = 1$, large amplitudes of Δu_x appear around the bottom of the sliding layer, while Δu_x at the top are negligible. It is found that the distribution of Δu_x becomes divergent from the shallow SBP approximation gradually with the increase of h/l_0. This is because any shear deformation $\partial\Delta u_x/\partial y$ within the sliding layer is ignored in the theoretical analysis. This is verified through a case with an enhanced stiffness ratio of $E/\tau_p = 10000$, where the deformation pattern of the sliding layer becomes close to the assumption of no shear deformation as shown in Fig. 5d. Although Δu_x above the pre-softened zone is varied with depth, the profile above the process zone is almost uniform. Compared with Fig. 5c, the discrepancy between the FE results and the shallow approximation becomes significantly narrower.

The process zone lengths ω are indicated in Fig. 5 as well. The ω is found to be influenced by h/l_0 and the displacement pattern within the sliding layer, although ω is irrelevant with l_0 in the analytical solution. As h/l_0 increases, ω/h is decreased from 0.99 to 0.72, while the analytical values remain 2.06 by Eq. (11). Note that except for the hypothetical case with $E/\tau_p = 10000$, none of the values of ω meet the requirement of the process zone approach ($h \ll \omega < l$) or other analytical approaches ($\omega \ll h \ll l$). This further proves the limitation of the existing analytical SBP methods for the cases with a shear band buried deeply.

The vertical distributions of Δu_x for the shallow and deep conditions are compared in Fig. 6 with three typical profiles: the middle of the pre-softened zone ($x/h = 0$), the interface between the pre-softened and process zones ($x/h =$ -0.5 l_0), and the interface between the process and elastic zones ($x/h = -(0.5\ l_0 + \omega)$). For the shallow condition, the vertical displacement distribution is almost uniform along the depth, with the average net displacement $\Delta\overline{u}_x$ (average value of Δu_x along the depth) close to $\Delta\delta$. For the deep condition, the variation of Δu_x along the depth is significant, resulting in $\Delta\overline{u}_x$ much smaller than $\Delta\delta$ at $x/h = 0$ and $-0.5\ l_0$, and larger than $\Delta\delta$ at $x/h = -(0.5\ l_0 + \omega)$. As a result, the stress $\Delta\overline{\sigma}_x$ calculated by Eq. (7) deviates from the physical conditions.

To further interpret this discrepancy, the lateral distributions of displacements, $\Delta\overline{u}_x$ and $\Delta\delta$, and the stress profiles, $\Delta\overline{\sigma}_x$ and $\Delta\tau$, along the slope for the shallow ($h/l_0 = 0.05$) and deep conditions ($h/l_0 = 1$), are compared with the analytical solutions in Fig. 7. For the shallow condition, the distribution of $\Delta\overline{u}_x$ and $\Delta\delta$ are close to the analytical solution, especially within the pre-softened zone. A clear discrepancy is found in the shear stress profile as shown in Fig. 7e. This is because the analytical solution overestimates the length of process zone and underestimates the $\Delta\overline{u}_x$ above the elastic zone. In turn, for FE analyses, the shear stress within the process zone decreases faster due to a shorter process zone, reducing the mobilized resistance force, which is then compensated by the larger shear stress and hence additional resistance force mobilized within the elastic zone. This discrepancy in the stress profile shows little effect on the final failure criterion under the shallow condition, as the critical values of $\tau_{g,cri}$ to trigger catastrophic SBP for both analytical and FE results are 28.5 kPa.

For deep conditions, the discrepancies of displacement and stress profiles between FE and analytical results become remarkable. Compared with the shallow displacement pattern, the pre-softened zone requires a larger $\Delta\delta$ to mobilize the sliding layer to move a similar $\Delta\overline{u}_x$. Consequently, the soil in a deeper shear band is more prone to being softened and reaching the critical condition for catastrophic SBP. The key is the $\Delta\delta$ at the interface between the pre-softened and process zones, which controls whether the soil strength at the interface is softened lower than current τ_g and hence provides the additional driven force. As shown in Fig. 7a and b, for the shallow condition, the analytical and FE values of $\Delta\delta$ at the interface are almost the same, while the FE value of $\Delta\delta$ at the interface are significantly larger than the analytical value for the non-shallow condition. The FE and analytical values of $\tau_{g,cri}$ corresponding to this critical condition are 52.5 and 56.6 kPa, respectively, representing an error of 7%.

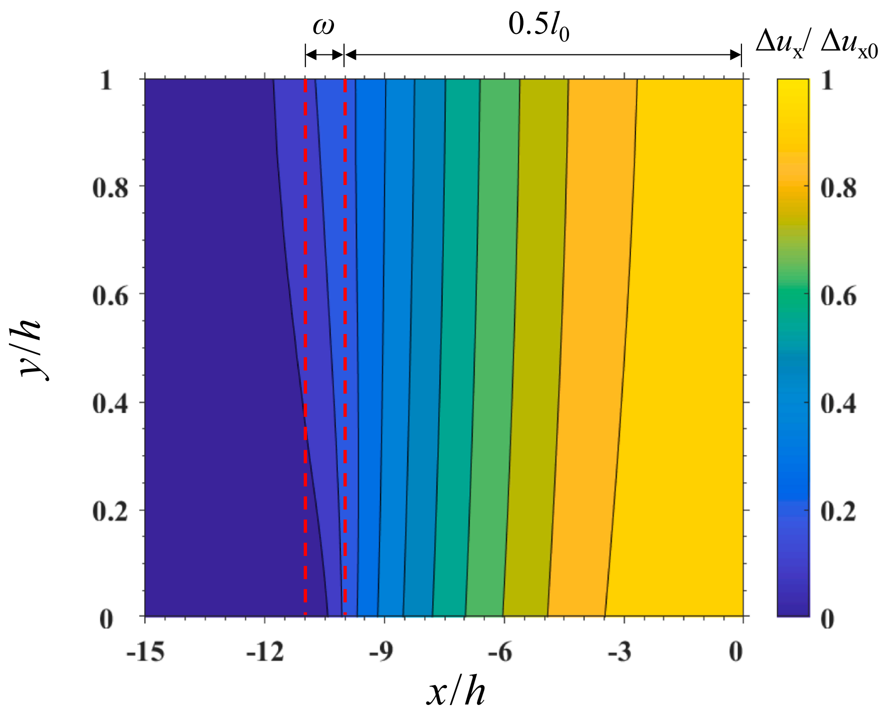

(a) $h/l_0 = 0.05$, $\Delta u_{x0} = 0.84$ m

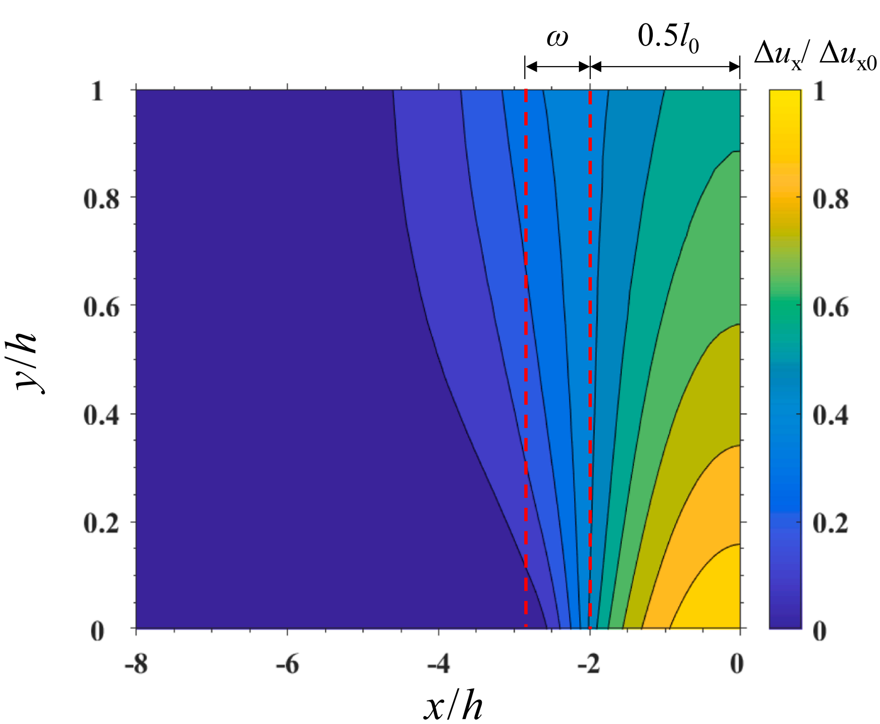

(b) $h/l_0 = 0.25$, $\Delta u_{x0} = 0.25$ m

Fig. 5. Distributions of normalized net displacement Δu_x at the critical condition for catastrophic propagations.

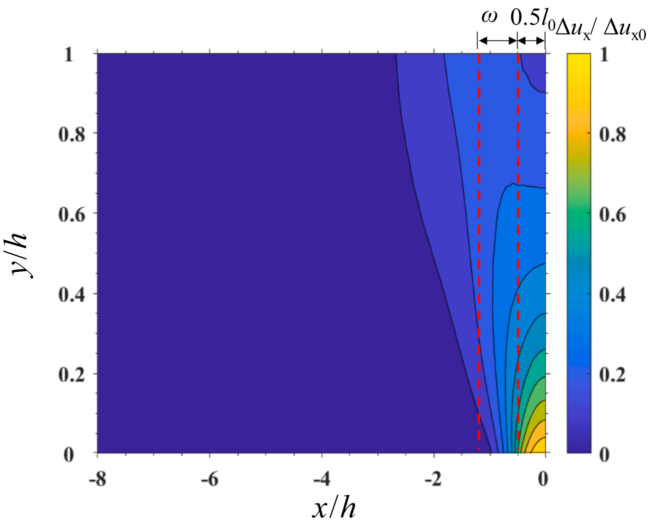

(c) $h/l_0 = 1$, $\Delta u_{x0} = 0.11$ m

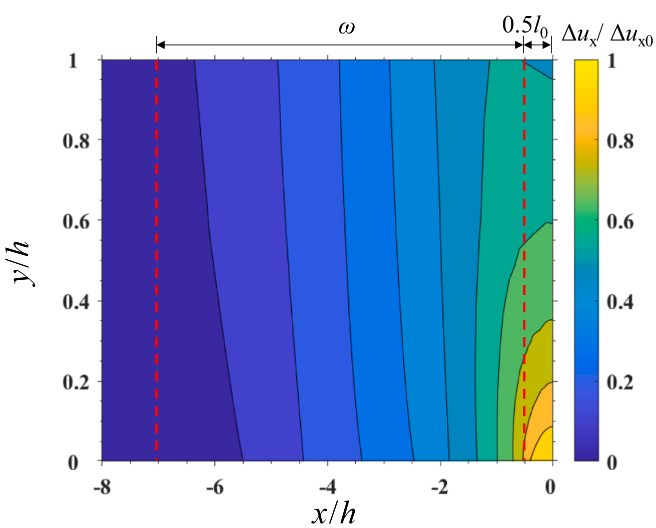

(d) $h/l_0 = 1$, $E/\tau_p = 10000$, $\Delta u_{x0} = 0.01$ m

Fig. 5. (*continued*).

The four cases investigated above reveal the transition from the shallow to non-shallow displacement pattern. The analytical failure criteria based on the shallow SBP approximation are proved to overestimate the slope stability under non-shallow SBP displacement patterns. To quantify this error, a correction factor, α, is proposed as

$$\alpha = \frac{\tau_{g,cri}}{\tau_{g,cri}^{ana}} \tag{14}$$

where $\tau_{g,cri}$ is the numerical value of τ_g at the critical condition for catastrophic SBP, and $\tau_{g,cri}^{ana}$ is the analytical value. For linear strength degradation rules under static conditions, the expression of $\tau_{g,cri}^{ana}$ is given by Eq. (10).

The transition of displacement pattern is highly related to the aspect ratio of the depth and length of the shear band, which consists of the pre-softened and process zones. In the subsequent analyses, the influences of the two zones on the correction factor are discussed respectively.

3.2. The influence of the pre-softened zone

Fig. 8a presents the correction factor α against h/l_0, where h/l_0 ranges between 0.025 and 3 with h fixed at 50 m. The correction factor is close to unity for $h/l_0 < 0.067$, and gradually decreased with increasing h/l_0, followed by a minimal rise when $h/l_0 > 1$. Therefore, one may set $h/l_0 = 0.067$ as the threshold value for shallow and non-shallow SBP conditions. The analytical failure criterion overestimates the slope stability when $h/l_0 > 0.067$. The slight increase of α with $h/l_0 > 1$ is due to that the $\tau_{g,cri}$ to trigger landslide is already very close to τ_p, resulting in a very small change of $\Delta\tau$ within the process zone. This compensates for the direct effect of the decrease in l_0 on the α.

The correction factor α is also affected by the reduced shear strength τ_0 within the pre-softened zone, as shown in Fig. 8b. For cases with $h/l_0 = 1$, the α is increased linearly from 0.89 to 0.97 as τ_0/τ_p ranging between 0.1 and 0.67. Low values of τ_0/τ_p could be met with an initiation history of accumulated excess pore pressure. As indicated in Fig. 7e and f, the stress profile of the shear band is limited between τ_0 and τ_p. When

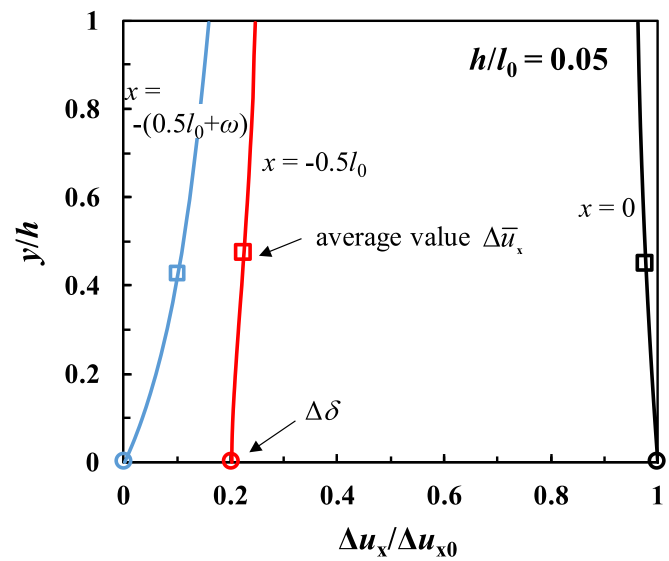

(a) shallow condition

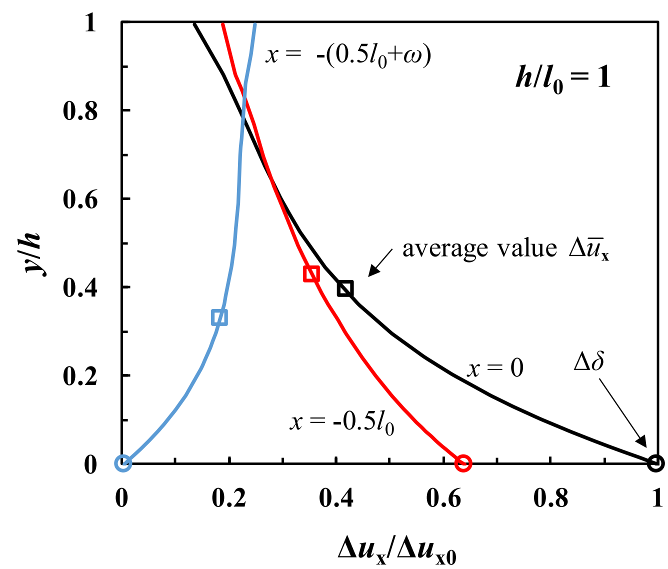

(b) deep condition

Fig. 6. Vertical distributions of normalized net displacement Δu_x.

the ratio τ_0/τ_p is decreased, the change of $\Delta\tau$ within the process zone becomes more significant, facilitating the larger shear deformation within the sliding layer and then mobilizing the non-shallow pattern.

3.3. The influence of the process zone

The length and the stress profile of process zone depend on the average Young's modulus E, thickness h of the sliding layer, the undrained shear strength ratio k, soil sensitivity S_t and the plastic shear displacement to residual δ_r^p of the weak layer. Fig. 8 shows the effects of these parameters on the correction factor α and the process zone length ω with $h/l_0 = 1$ taken as an example for non-shallow SBP. The parameters used are listed in Table 1.

The values of α and ω are sensitive to δ_r^p and h. As δ_r^p is increased from 0.05 to 0.8 m, α is increased from 0.85 to 0.98 and ω/h from 0.25 to 2.05. When h ranges from 10 to 200 m, α decreases from 0.98 to 0.85 and ω/h from 2.68 to 0.24. Despite $h/l_0 = 1$, the error caused by shallow SBP approximation can be ignored when $\omega/h \geq 2$, corresponding to $\delta_r^p > 0.8$ m or $h < 10$ m. The values of α and ω are moderately sensitive to E/τ_p and S_t. For all cases, $\omega/h \leq 1.5$ and $\alpha \leq 0.96$. Although not presented in Fig. 9, the value of α remains constant with k changing from 0.15 to 0.35, indicating that the magnitude of τ_p has no straightforward influences on the displacement pattern when E/τ_p and S_t are fixed.

It is evident from Fig. 9 that the parameters α and ω/h are not decoupled, as α is influenced by the shear stress profile of the process zone. Hence, the characteristic length of shear band l_u expressed by Eq. (9), a function of the above factors, is attempted to quantify their combined effects on α. As shown in Fig. 10, the influence of these factors on α can be represented well by h/l_u as all the cases can be fitted with a unique curve.

3.4. Empirical correction equation and its verification

Figs. 8 and 10 demonstrate that the correction factor α exhibits a nearly linear relationship with h/l_0, h/l_u and τ_0/τ_p, respectively, indicating that the error caused by the shallow SBP approximation may be corrected through a simple empirical equation. A characteristic depth parameter Λ is defined by combining the three factors as

$$\Lambda = \frac{(1 - \tau_0/\tau_p)h}{l_0 + 3l_u} \tag{15}$$

Note that the analytical value of process zone length ω is around $1.4l_u$ $-1.5l_u$ based on Eq. (11). Thus, the physical meaning of $h/(l_0 + 3l_u)$ can be interpreted as the aspect ratio of the depth to the theoretical length of shear band, which includes the pre-softened zone and the process zones at the two ends. The correction factor α against Λ for the above cases is plotted in Fig. 11. A bilinear expression is observed: α is roughly equal to unity as $\Lambda \leq 0.04$, and α is decreased linearly with Λ as $\Lambda > 0.04$:

$$\begin{cases} \alpha = 1 & \Lambda \leqslant 0.04 \\ \alpha = 1 - 0.8(\Lambda - 0.04) & 0.04 < \Lambda < 0.56 \end{cases} \tag{16}$$

The former condition, $\Lambda \leq 0.04$, represents where the shallow SBP approximation is satisfied, while the latter indicates the correction under non-shallow SBP. The range of applicability of Eq. (16), $0 < \Lambda < 0.56$, is determined subsequently.

Three groups of tests were designed to examine the robustness of Eq. (16): (I) $\Lambda < 0.56$ and $h/l_0 \leq 1$; (II) $\Lambda < 0.56$ and $h/l_0 > 1$; and (III) $\Lambda > 0.56$. Seven dominant factors investigated above are varied, as listed in Table 2. Group (I), consisting of the orthogonal combinations of common parameter values with $h/l_0 \leq 1$, covers the vast majority of possible slope failure conditions. The predicted correction factors for group (I) are in good agreement with the FE results in Fig. 12, showing the good potential of Eq. (16) in slope assessment. The FE results deviate from the predicted results for group (II) with $h/l_0 > 1$, however, Eq. (16) provides a lower bound of α. In addition, for submarine landslides with low inclination, it is reasonable to believe that catastrophic failures are rarely triggered by a very short pre-softening zone. To further explore the value of α when Λ continues to increase, a series of extreme slope failure conditions, which are virtually impossible to encounter in engineering practice, are presented in group (III). It is found that even the minimum value of α is>0.5 as shown in Table 2 and Fig. 12. Thus, $\alpha = 0.5$ is suggested as the empirical solution when $\Lambda > 0.56$.

A new dimensionless empirical failure criterion in terms of $\tau_{g,cri}$ is derived by combining Eqs. (10), (15) and (16), as

$$\widehat{\tau}_{g,cri} = \alpha \frac{\widehat{l}_0 \widehat{\tau}_0 + 2}{\widehat{l}_0 + 2} \tag{17}$$

$$\widehat{\tau}_{g,cri} = \tau_{g,cri}/\tau_p, \widehat{l}_0 = l_0/l_u, \widehat{\tau}_0 = \tau_0/\tau_p \tag{18}$$

Substituting Eq. (16) into Eq. (17), the empirical failure criterion in terms of l_{cri} can be given by

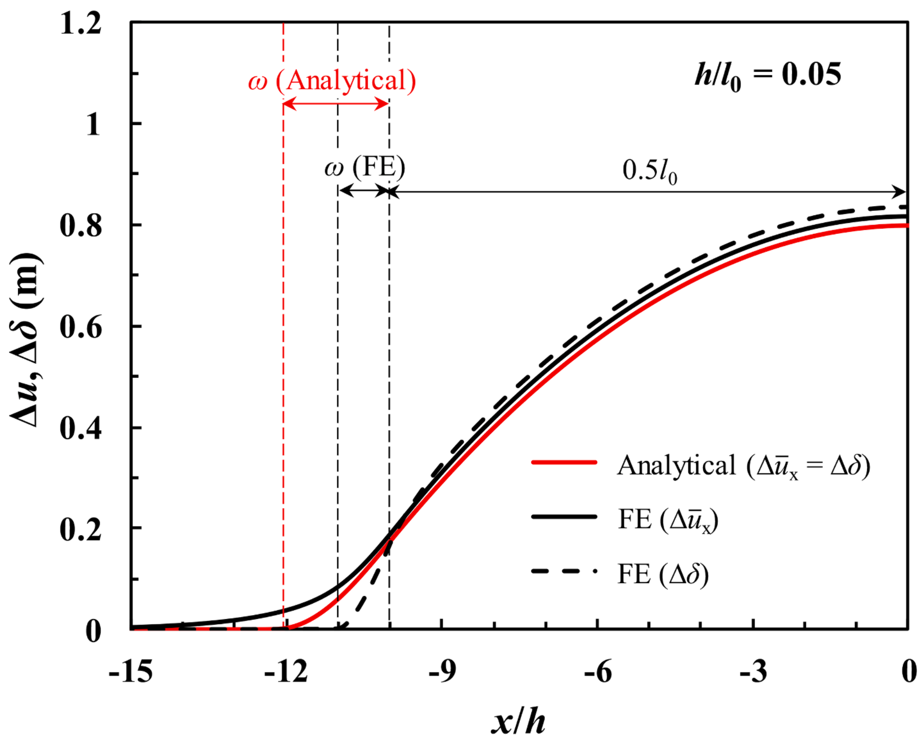

(a) Δu and $\Delta\delta$ profile with h/l_0=0.05

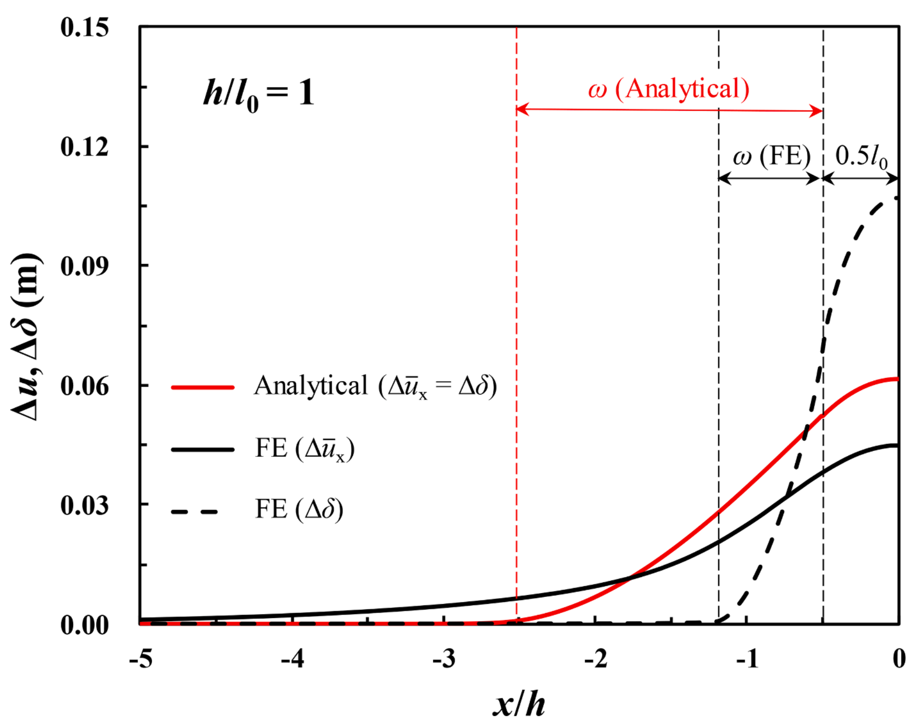

(b) Δu and $\Delta\delta$ profile with h/l_0=1

Fig. 7. Responses at the critical conditions for catastrophic SBPs at different relative depths.

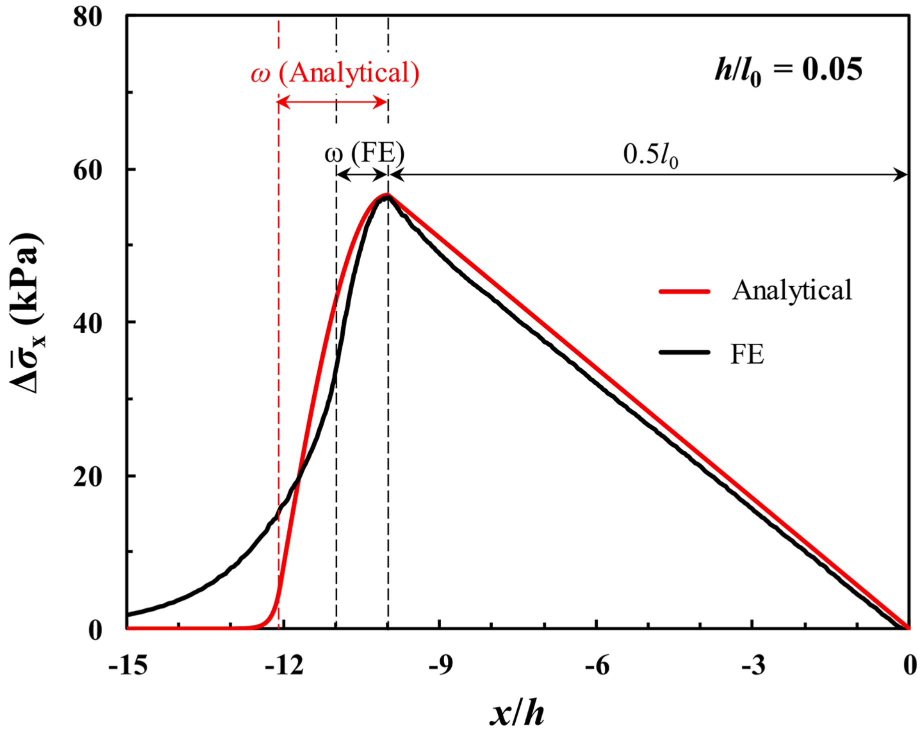

(c) $\Delta\bar{\sigma}_x$ profile with h/l_0=0.05

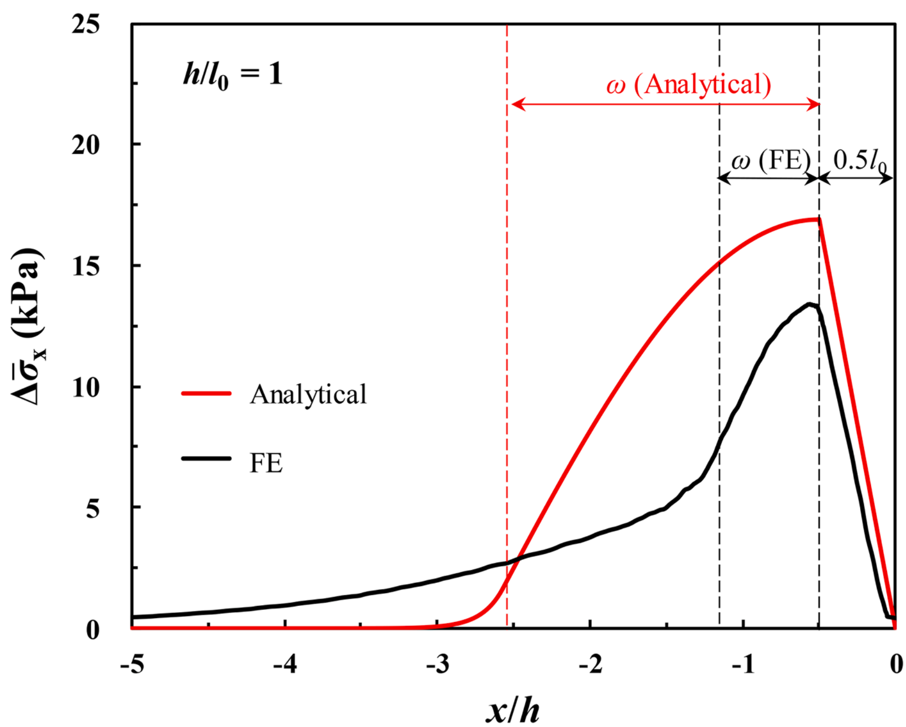

(d) $\Delta\bar{\sigma}_x$ profile with h/l_0=1

Fig. 7. (*continued*).

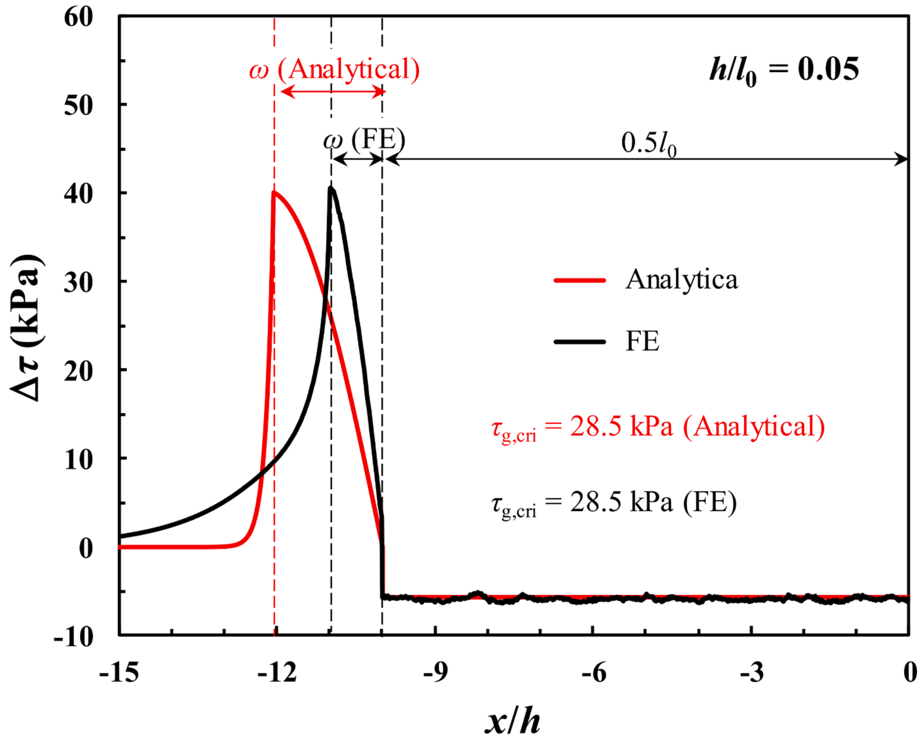

(e) $\Delta\tau$ profile with h/l_0=0.05

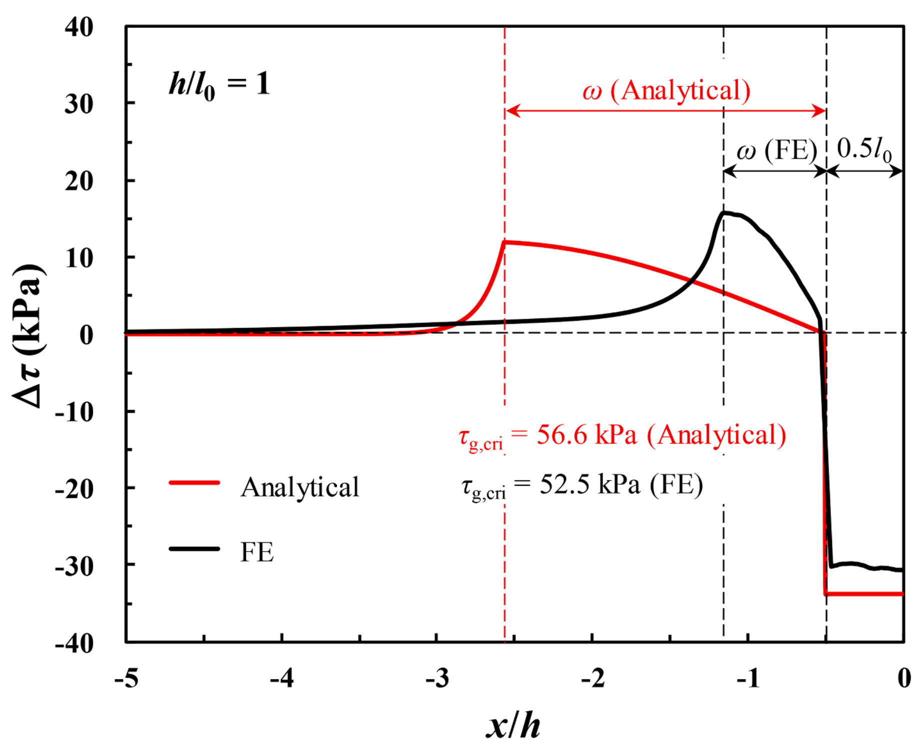

(f) $\Delta\tau$ profile with h/l_0=1

Fig. 7. (*continued*).

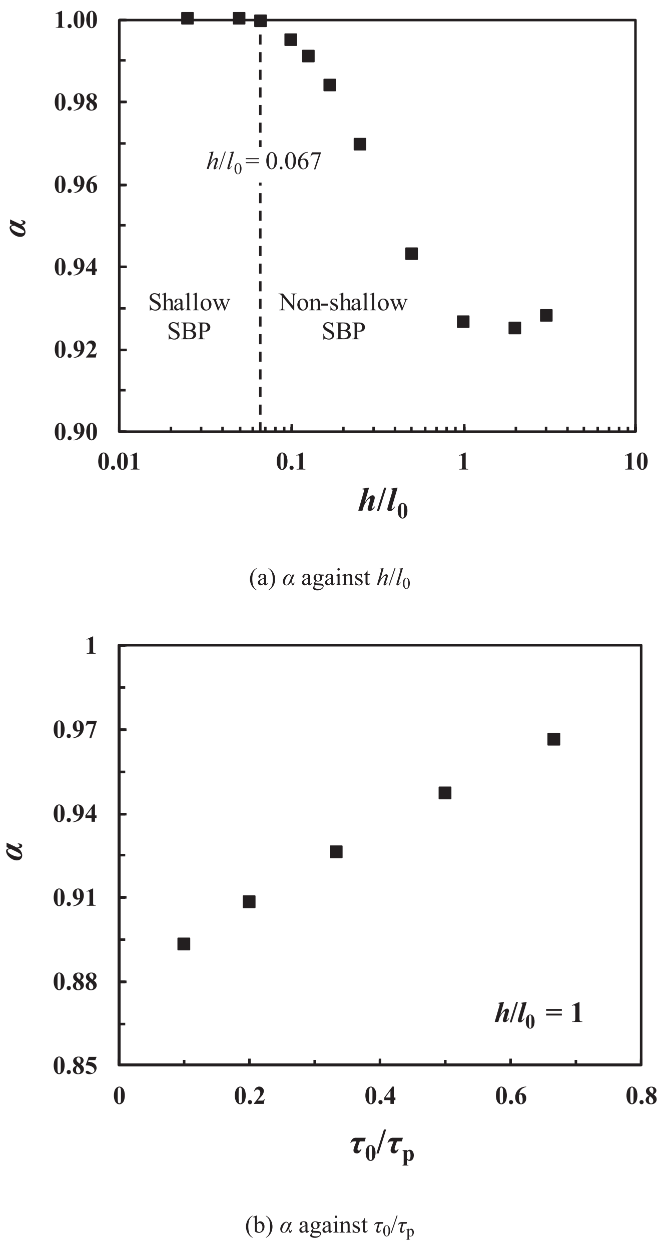

(a) α against h/l_0

(b) α against τ_0/τ_p

Fig. 8. The influences of the pre-softened zone on the correction factor α.

$$\begin{cases} \widehat{l}_{cri} = \dfrac{2(1-\widehat{\tau}_g)}{\widehat{\tau}_g - \widehat{\tau}_0} & \Lambda \leqslant 0.04 \\ \widehat{l}_{cri} = \dfrac{a + \sqrt{a^2 + 4(\widehat{\tau}_g - \widehat{\tau}_0)b}}{2(\widehat{\tau}_g - \widehat{\tau}_0)} & 0.04 < \Lambda < 0.56 \end{cases} \tag{19}$$

$$\begin{aligned} &\widehat{l}_{cri} = l_{cri}/l_u, a = (3 - 0.8\widehat{h}(1-\widehat{\tau}_0))\widehat{\tau}_0 + 2 - 5\widehat{\tau}_g, \\ &b = 6(1-\widehat{\tau}_g) - 1.6\widehat{h}(1-\widehat{\tau}_0), \widehat{h} = h/l_u, \widehat{\tau}_g = \tau_g/\tau_p \end{aligned} \tag{20}$$

Note that $a^2 + 4(\widehat{\tau}_g - \widehat{\tau}_0)b < 0$, where the solution of Eq. (19) is unavailable as the value under the square root is < 0, suggests a condition where the $\widehat{\tau}_g$ value is so high that l_{cri} approaches zero. Although the exact close form of failure criteria in terms of $\tau_{g,cri}$ and l_{cri} are non-available, Eqs. (17) and (19) provide an empirical solution.

4. Example application: The Storegga Slide

A case study for a section of the Storegga Slide in the Ormen Lange field is conducted to illustrate the application of the empirical failure criterion. The initial instability of the Storegga Slide is believed to be triggered at the lower and steeper part of the slope by regional high excess pore pressure due to rapid deposition or hydrate decomposition, followed by subsequent progressive failure (Kvalstad et al., 2005a; Vanneste et al., 2014). Nowadays, excess pore pressure of 200 kPa is still measured at a soil depth of 200 m in a location close to the headwall of the Ormen Lange field (Strout and Tjelta, 2005). Here, the analysis of the Storegga Slide is simplified as a plane strain problem, as depicted in Fig. 13.

Following the case study of Kvalstad et al. (2005a), slope geometry and soil parameters are determined below. The slope is simplified as a planar one with a weak layer at depth of 200 m. The slope inclination θ is 2° measured from the reconstructed slope surface. The soil properties were determined based on the in-situ cone penetration tests and laboratory tests in Kvalstad et al. (2005b): the average submerged density is $\rho' = 900$ kg/m^3, the shear strength ratios of the sliding mass and the weak layer are $k = 0.3$ and 0.2, respectively, and the soil sensitivity S_t of the weak layer is 5. The plastic shear displacement δ_r^p to residual state is set to 0.2 m, which is typical for marine sensitive clays. The ratio of average plane strain Young's modulus E_{ps} of the sliding layer to its average shear strength is estimated as a typical value of 300. Linear strain-softening relationship of the shear band is adopted. Excess pore pressure Δu is assumed to be uniformly distributed along the entire slope except for the pre-softened zone. The shear strength of the pre-softened zone is fully reduced to τ_0 lower than τ_g, which could be caused by hydrate dissociation or concentration of high excess pore pressure. The peak undrained shear strength of soil considering the reduction by excess pore pressure is estimated by (Kvalstad et al., 2005a)

$$\tau_p = k(1 - r_u)\rho' gz \tag{21}$$

where $r_u = \Delta u/\rho' gz$ is the excess pore pressure ratio. To ensure the shear band is extendable along the weak layer, the shear stress by gravity at the weak layer should be larger than the residual strength ($\tau_g > \tau_r = \tau_p/S_t$), so that r_u is expected to be > 0.13 according to Eq. (21). The parameters used in the assessment of slope stability are summarized in Table 3.

Two scenarios are considered: (a) the strength of the pre-softened zone τ_0 is decreased to 0 corresponding to the most unfavorable condition, while r_u outside the pre-softened zone is varied; and (b) r_u outside the pre-softened zone is maintained at 0.3, which might be a common value at the onset of the Storegga Slide, but explore the effect of τ_0. The corresponding critical lengths l_{cri} of pre-softened zone are derived based on the analytical and empirical failure criteria, i.e. Eqs. (8) and (19), respectively, as shown in Fig. 14.

For scenario (a), the values of l_{cri} at $r_u = 0.13$ from Eqs. (8) and (19) are 845.5 and 715.7 m, respectively, indicating the giant Storegga Slide can be initiated with a rather limited pre-softened zone. Eq. (19) accounting for the deep buried shear band provides a more conservative estimate (about 18% shorter in terms of l_{cri}) than Eq. (8). The value of l_{cri} decreases with the increase of r_u, and the relative difference between the l_{cri} from the two criteria becomes more significant. When $r_u = 0.6$, the analytical value of l_{cri} is 274.1 m, compared with 106.5 m from the proposed criterion.

For scenario (b), the values of l_{cri} from Eqs. (8) and (19) when $\tau_0/\tau_p = 0$ are 638.8 and 464.7 m, respectively. The values of l_{cri} from both criteria increase exponentially with the increase of τ_0/τ_p. Fig. 14b shows that the catastrophic SBP under non-shallow conditions is highly likely to occur at $\tau_0/\tau_p \leq 0.22$, where the criterion proposed in this study is more conservative for assessing the failure.

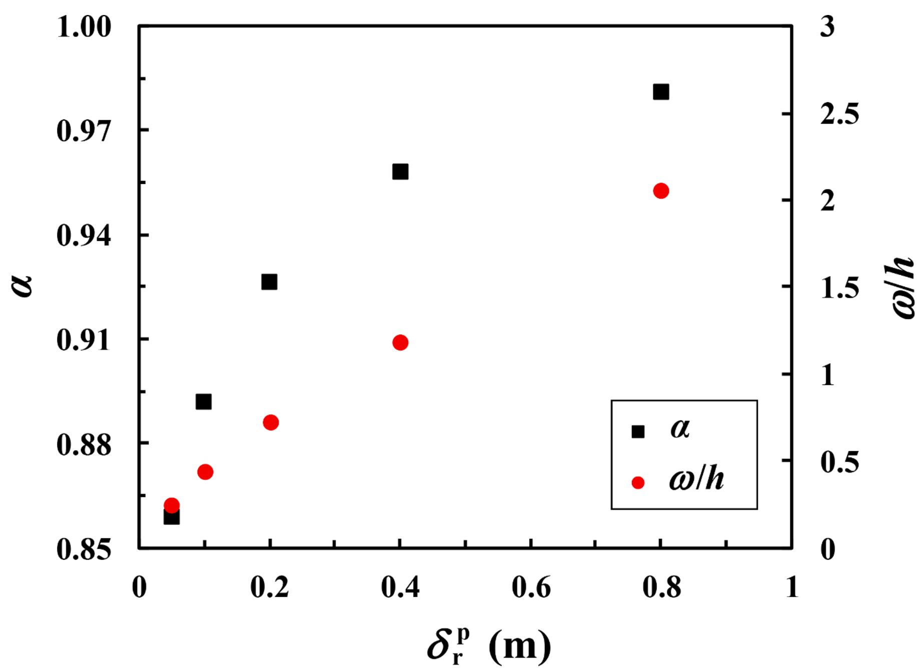

(a) the plastic shear displacement to residual δ_r^p

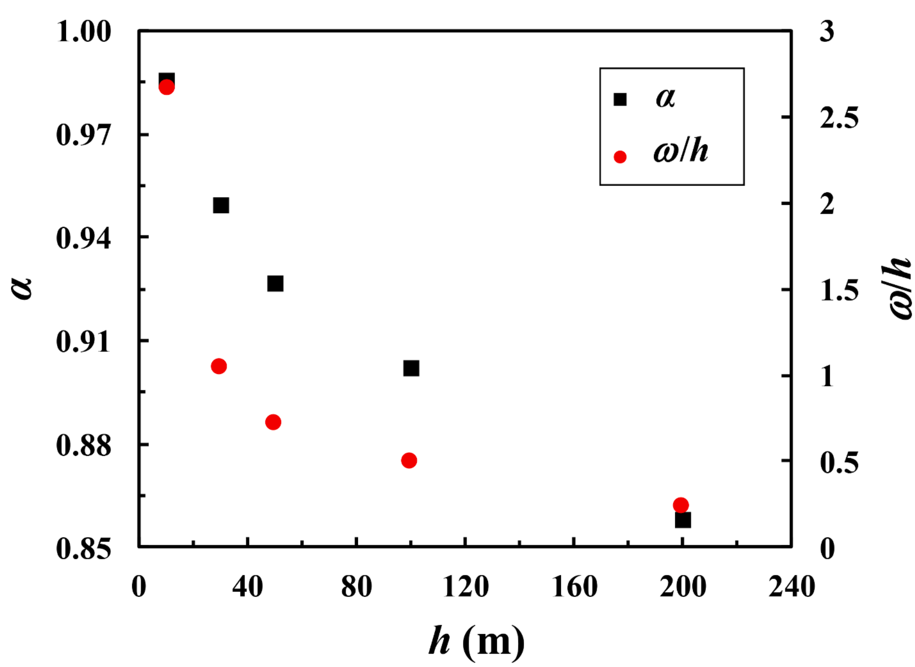

(b) the thickness of sliding layer h

Fig. 9. The influence of process zone properties on correction factor α and process zone length ω.

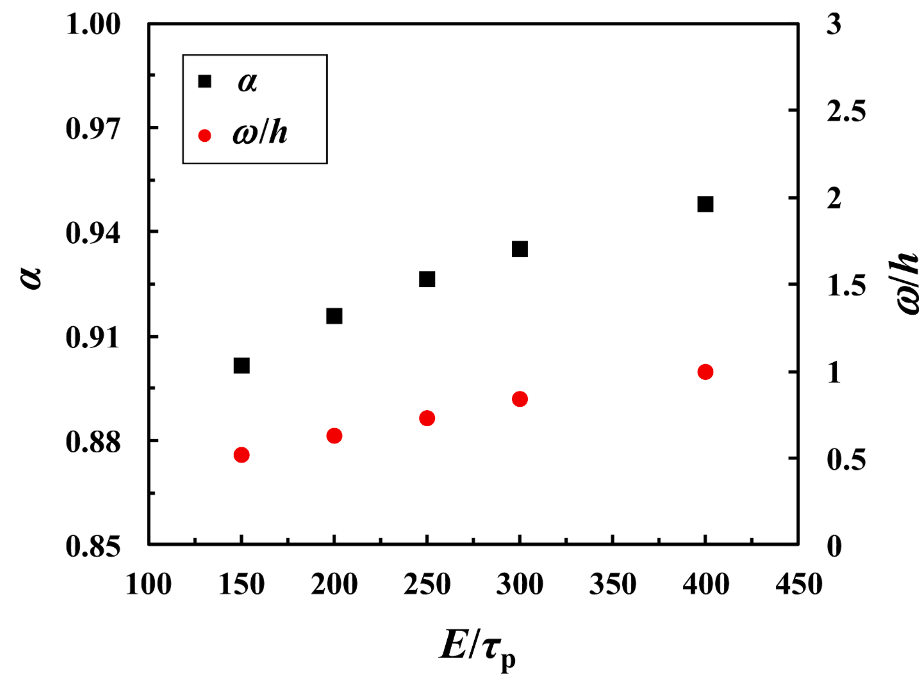

(c) the stiffness ratio of sliding layer E/τ_p

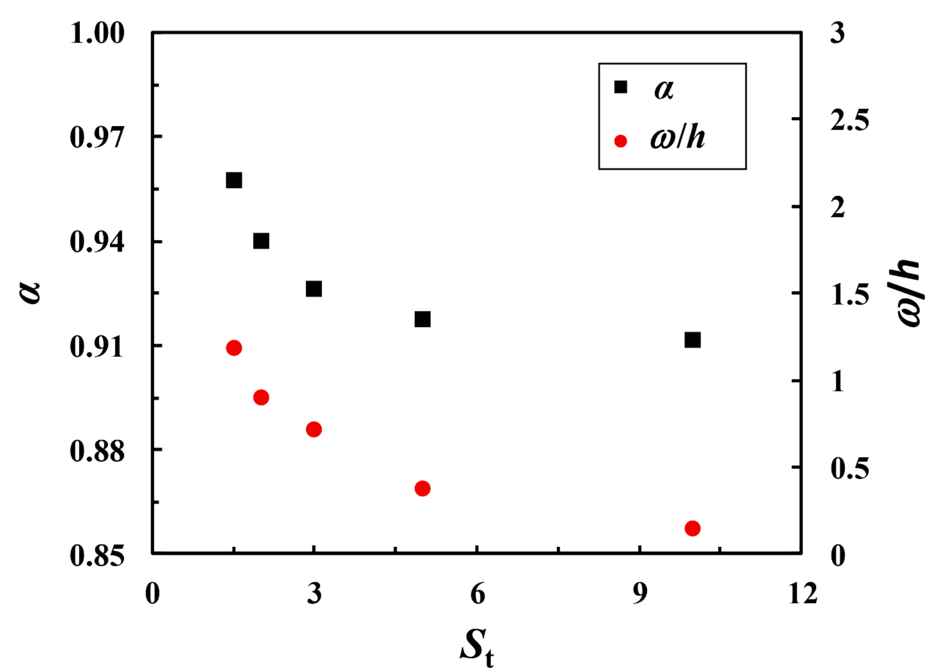

(d) the sensitivity of shear band S_t

Fig. 9. (*continued*).

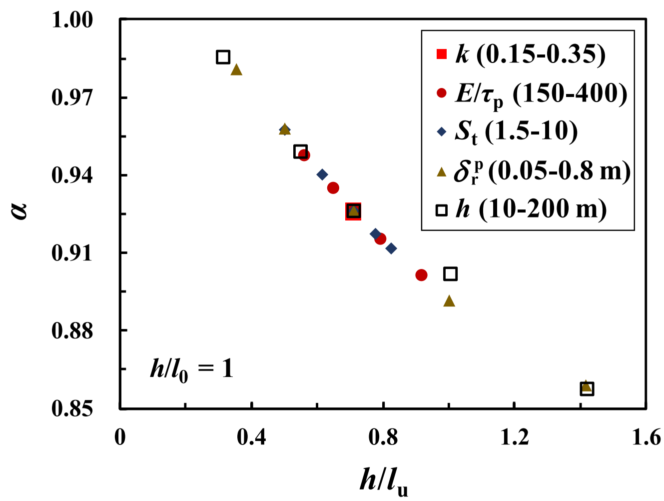

Fig. 10. Relationship of normalized process zone properties h/l_u and correction factor α.

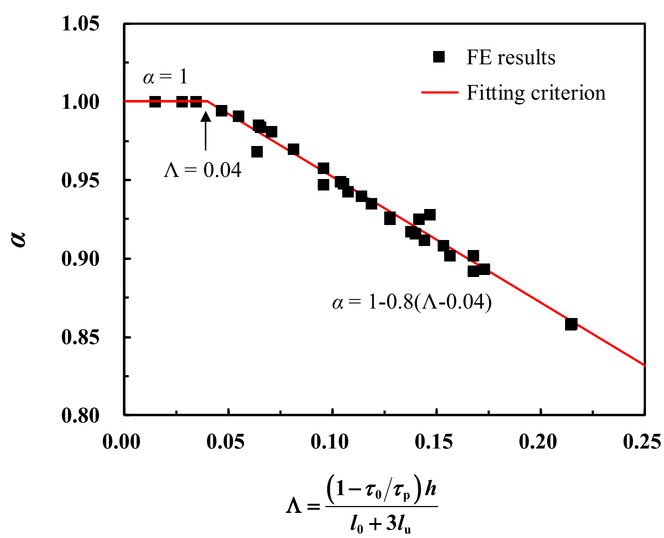

Fig. 11. The correction factor α against the characteristic depth parameter Λ.

Note that the limit equilibrium analysis assumes that the failure of the entire slip surface occurs simultaneously, implying very low shear strength of soils along several to tens of kilometres for the Storegga Slide which is highly unlikely. In contrast, by considering the strain-softening, the proposed mechanism suggested that the Storegga Slide may be triggered by the shear band propagating from a much smaller initial failure zone (around half a kilometre) to the entire sliding surface. Maintaining simplicity for application, the proposed criterion presents a more reasonable failure mechanism.

5. Discussions

In the above sections, static FE analyses are conducted to explore the transition of displacement pattern between the shallow and non-shallow SBP conditions with a linear strain-softening response of the shear band. An empirical solution is proposed to access the slope stability for both shallow and non-shallow conditions. These studies are subsequently extended to account for SBPs against the different strain-softening relationships, and the inertia effect which considers the kinetic energy of the sliding layer due to the rapid formation of the pre-softened zone.

5.1. The influence of strain-softening relationship

The impact of the strain-softening relationship on the correction factor is investigated by adopting an exponential strength softening response of shear band, as shown in Fig. 2b. Note that the $\tau_{g,cri}^{ana}$ should be calculated by the failure criterion for exponential strength softening response (Zhang et al., 2015). The base cases with h/l_0 ranging from 0.05 to 3 are re-analysed using the constitutive relationship of weak layer expressed by Eq. (3). The corresponding characteristic length of the shear band for exponential softening response is given by

$$l_u = \sqrt{2E_{ps}h\delta_{95}^{p}/3(\tau_p - \tau_r)} \tag{22}$$

The plastic shear displacement δ_{95}^{p} to achieve 95% reduction in shear strength is set to 1.5 δ_r^p to ensure that the value of l_u is the same as that of linear strength degradation response.

Fig. 15a shows the comparison of the correction factor between the linear and exponential degradations. The α for exponential and linear degradations are close to each other when $h/l_0 < 1$, while the former is lower when $h/l_0 \geq 1$, indicating a more pessimistic case. This is due to the strain-softening rate of exponential degradation being higher than that of linear degradation with $h/l_0 \geq 1$, resulting in a shorter process zone and less feasible shallow SBP approximation. For example, ω/h at $h/l_0 = 1$ for exponential and linear degradations are 0.56 and 0.72, respectively. Due to a narrower process zone with the same l_u, the characteristic depth parameter Λ for exponential degradation is justified by reducing the contribution of l_u, as

$$\Lambda = \frac{(1 - \tau_0/\tau_p)h}{l_0 + 2l_u} \tag{23}$$

Compared with the expression of Eq. (15), the value of Λ becomes larger under the same conditions, indicating a more significant deep displacement pattern. Without modifying the relationship of α and Λ by Eq. (16), the empirical correction equation is shown in Fig. 15b. Although α deviates from the correction equation as $\Lambda \geq 0.18$, the simple correction equation remains conservative.

5.2. the influence of the inertia effect

The influence of the inertia effect on the correction factor is investigated through dynamic FE analyses. The pre-softened zone is assumed to be formed instantaneously. Then, the kinetic energy of the sliding layer is accumulated initially and subsequently dissipated to promote the SBP, which results in further development of the process zone. The $\tau_{g,cri}^{ana}$ to trigger the catastrophic SBP under dynamic conditions is calculated by the dynamic failure criteria in Zhang et al. (2016). Fig. 16 shows the variation of α with h/l_0 ranging from 0.05 to 3 under dynamic and static conditions. The correction factors under the static and dynamic conditions are close to each other at $h/l_0 < 0.5$, while the dynamic one becomes higher as $h/l_0 \geq 0.5$. This can be attributed to the additional growth of the process zone in the dynamic analyses, which compensates for the error caused by the shallow SBP approximation. For simplification, Eq. (16) based on the static conditions can be applied to the dynamic conditions, providing a more conservative correction factor.

Table 2
Orthogonal tests designed.

Group	h/l_0	k	E/τ_p	S_t	δ_r^p(m)	τ_0/τ_p	h (m)	Λ	α by Eq. (16)	α by FE
I	1	0.15	150	10	0.05	0.1	200	0.528	0.61	0.66
	1	0.2	150	1.5	0.8	0.33	10	0.031	1.00	1.00
	1	0.35	250	10	0.2	0.1	50	0.195	0.88	0.87
	1	0.15	150	10	0.1	0.1	200	0.451	0.67	0.68
	1	0.2	250	10	0.05	0.33	200	0.351	0.75	0.80
	1	0.35	400	3	0.05	0.33	200	0.287	0.80	0.82
	0.25	0.15	150	10	0.05	0.1	200	0.192	0.88	0.91
	0.25	0.2	250	3	0.2	0.33	50	0.082	0.97	0.97
	0.25	0.35	150	3	0.8	0.1	10	0.049	0.99	1.00
	0.25	0.35	250	1.5	0.05	0.67	200	0.060	0.98	0.98
	0.1	0.15	250	10	0.05	0.33	10	0.049	0.99	0.99
	0.1	0.15	400	3	0.2	0.33	200	0.053	0.99	0.99
	0.1	0.2	150	3	0.05	0.67	50	0.028	1.00	1.00
	0.1	0.35	400	10	0.8	0.1	200	0.062	0.98	0.99
II	3	0.2	250	5	0.2	0.2	500	0.515	0.62	0.75
	3	0.15	250	3	0.2	0.33	50	0.147	0.91	0.94
	2	0.2	150	3	0.05	0.33	200	0.508	0.63	0.77
	2	0.2	150	10	0.05	0.33	200	0.557	0.59	0.80
	2	0.2	250	5	0.2	0.2	500	0.465	0.66	0.67
III	10	0.15	150	10	0.05	0.1	500	1.650	−0.29	0.53
	5	0.15	150	10	0.05	0.1	500	1.394	−0.08	0.52
	3	0.15	150	10	0.05	0.1	500	1.156	0.11	0.54
	2	0.15	150	10	0.05	0.1	500	0.952	0.27	0.57
	1	0.15	150	10	0.05	0.1	500	0.623	0.53	0.66

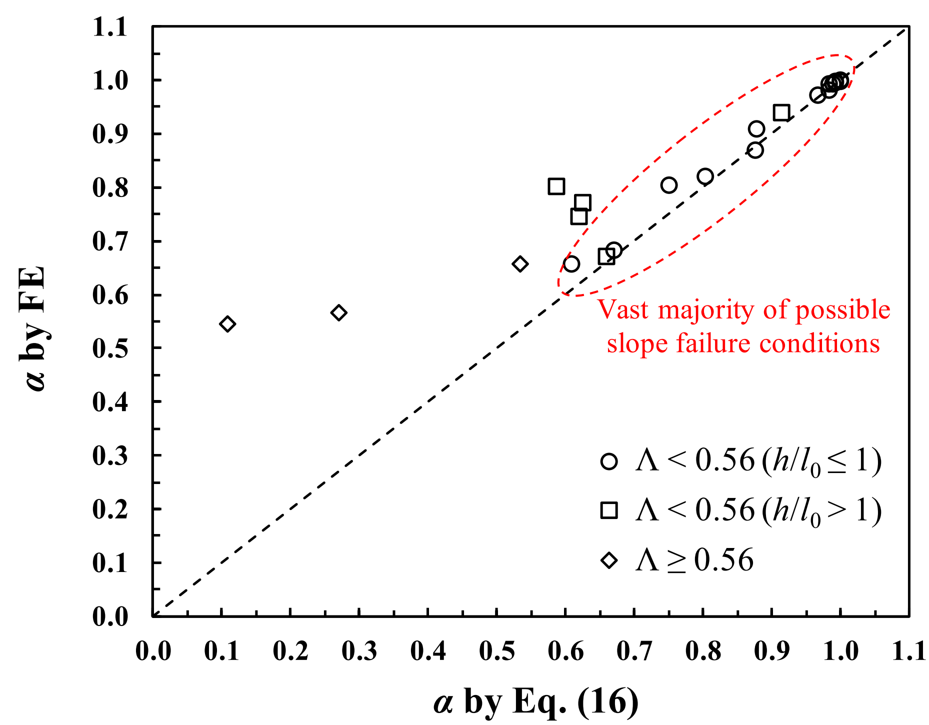

Fig. 12. Verification of the empirical correction equation by orthogonal tests.

6. Conclusions

Shear band propagation (SBP) methods are a promising tool to evaluate the progressive failure of submarine slopes. To obtain the analytical solution of failure criteria, the shallow SBP approximation, which assumes that the averaged displacement distribution of sliding layer along the depth is identical to the shear displacement of shear band, has been commonly adopted in the previous theoretical SBP analyses. However, this assumption is only valid when the length of initial shear band is much larger than its depth. In this study, finite element analyses are conducted to understand and quantify the errors induced by the shallow SBP approximation under non-shallow conditions. A simple empirical correction equation is proposed based on the finite element numerical investigation. The main conclusions of this study are summarized as follows.

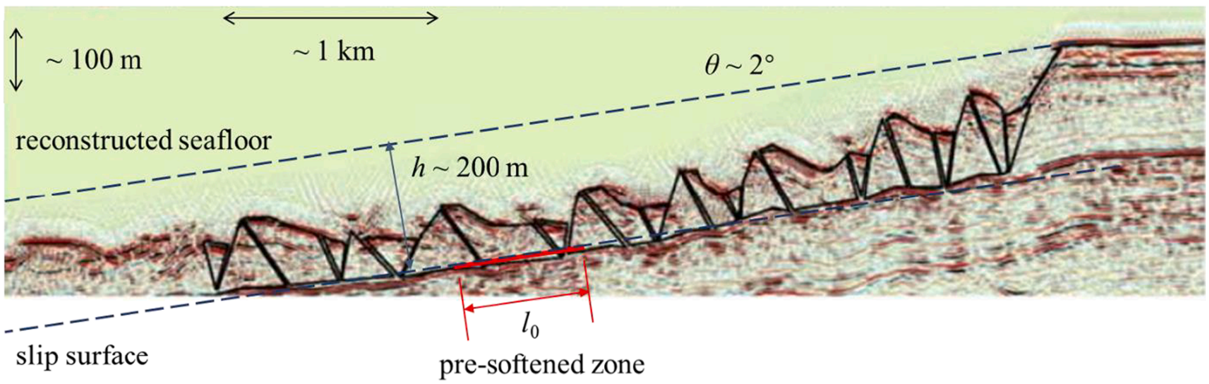

Fig. 13. Seismic profile of a section of the Storegga Slide which simplified as a planar slope in the analysis (modified from Kvalstad et al., 2005a).

Table 3
Historical study of the Storegga slide.

Parameters	the Storegga Slide
Slope angle θ	2°
Thickness of sliding layer h	200 m
Peak shear strength of weak layer τ_p	$360(1 - r_u)$ kPa
Average plane strain Young's modulus of sliding layer E_{ps}	$81(1 - r_u)$ MPa
Gravitational shear stress τ_g	62.8 kPa
Characteristic length of shear band l_u	106 m
Characteristic depth parameter Λ	0.17–0.39 for scenario (a) 0–0.21 for scenario (b)

(1) The shallow SBP approximation is reasonable when a slip surface is seated shallowly relative to the initial shear band length. For a deep slip surface, however, the lateral deformation of sliding layer is concentrated near the shear band and turns small as the soil depth becomes shallower. The existing analytical criteria based on shallow SBP approximation may significantly overestimate the slope stability under non-shallow conditions.
(2) A characteristic depth parameter, determined by the length and the strength ratio of initial fully softened zone, the thickness of sliding layer and soil properties, is proposed through Eq. (15) to distinguish between the shallow and non-shallow SBP conditions with a threshold value of 0.04. A bilinear empirical expression, Eq. (16), with a correction factor as a function of characteristic depth parameter is proposed to quantify the catastrophic SBP for both shallow and non-shallow conditions.
(3) The exponential softening response of shear band enlarges the error caused by the shallow SBP approximation compared with the linear strain-softening response, while the dynamic inertia, associated with the relatively rapid formation of an initial shear band, reduces this error.
(4) A case study of the Storegga Slide suggests the initial failure is likely triggered under the non-shallow SBP condition. The critical length of the initial fully softened zone for the giant failure could be as small as around half a kilometer with a basal shear surface at depth of 250 m.

It should be noted that, in most cases, the plane-strain (2D) analytical criterion for catastrophic shear band propagation along a deep-seated weak layer is conservative compared to the 3D scenario as the out-of-plane dimension of the pre-softened zone is assumed infinity. However, the shear band propagation is restrained to single direction and multi-directional propagation of shear band may induce additional driving forces under certain conditions as discussed in Zhang et al. (2022) for shallow SBP. It is therefore necessary to extend the study to investigate multi-directional SBP within a deep-seated weak layer.

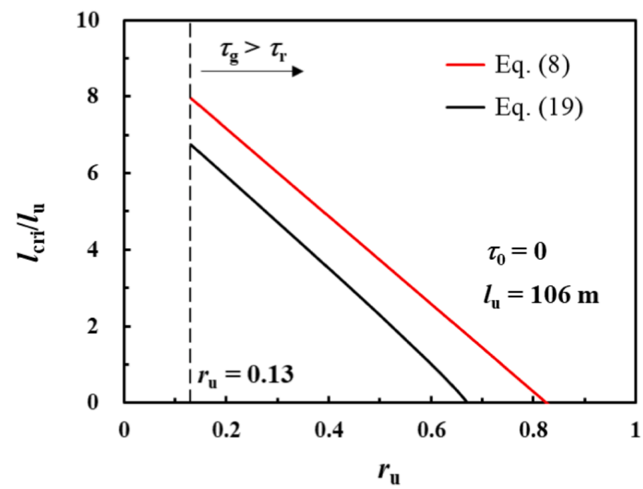

(a) excess pore pressure ratio r_u

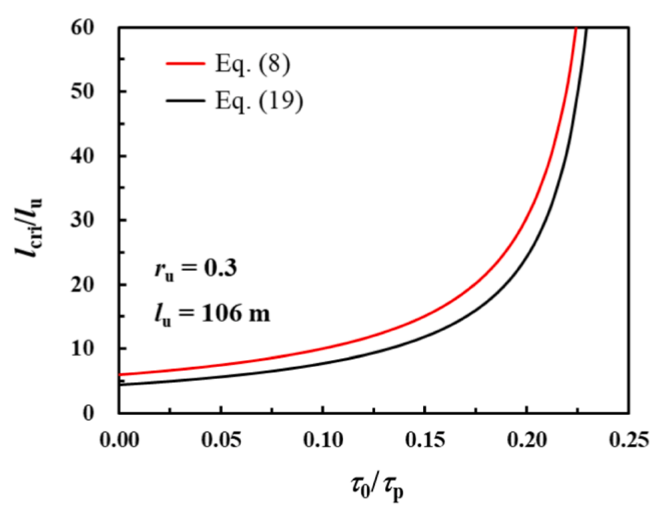

(b) reduced strength within the pre-softened zone τ_{r0}

Fig. 14. Comparison of the analytical and empirical failure criteria in terms of critical pre-softened zone length.

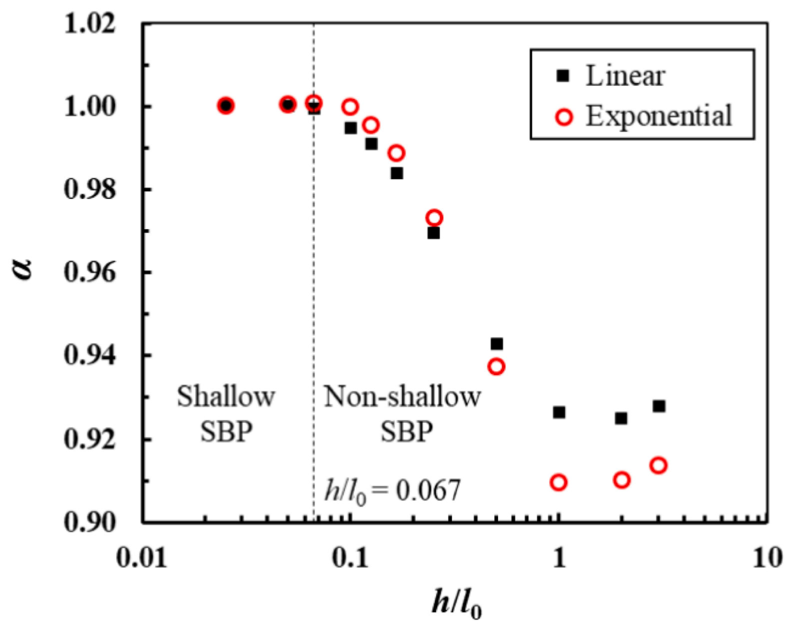

(a) correction factor α against h/l_0

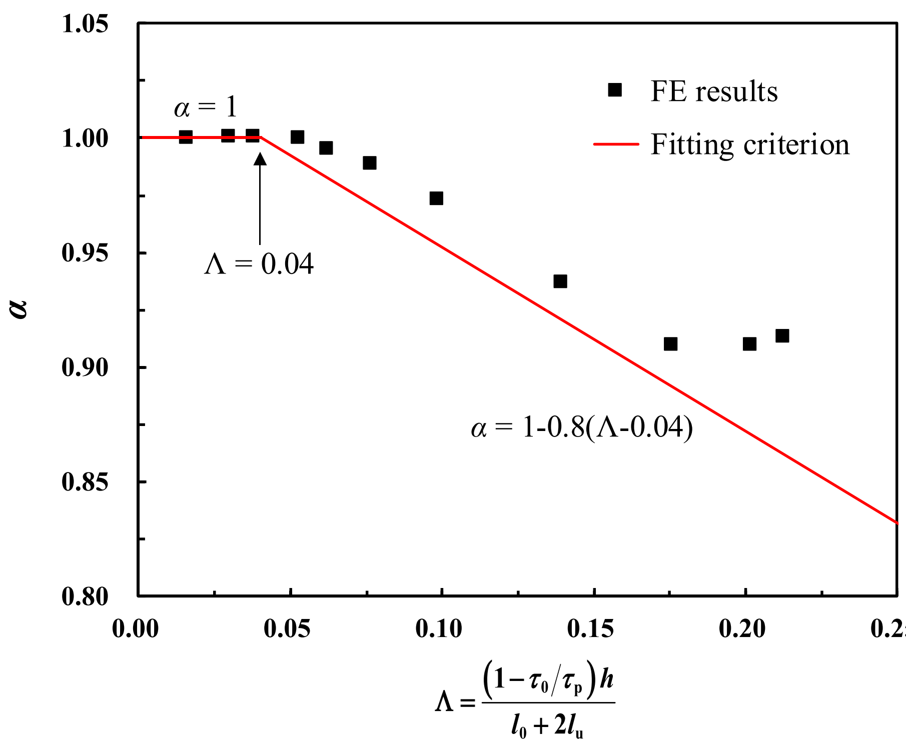

(b) empirical correction equation

Fig. 15. The influence of different strength degradations.

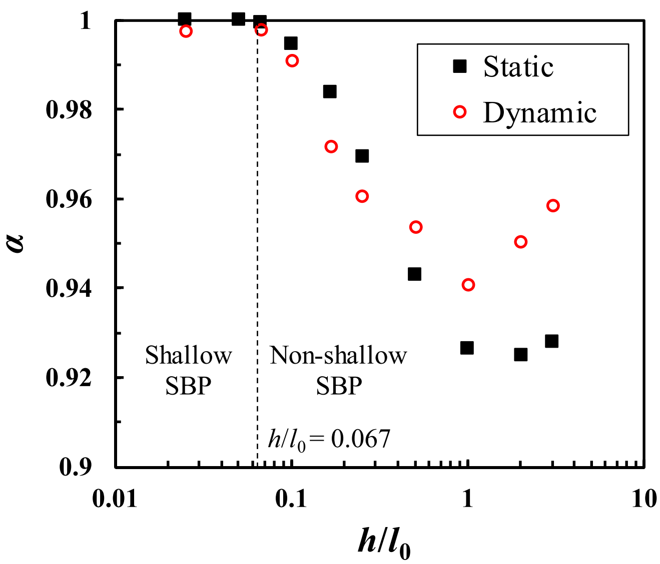

Fig. 16. The correction factor α against the relative depth h/l_0.

CRediT authorship contribution statement

Zhipeng Zhu: Writing – original draft, Investigation, Software, Data curation, Validation. **Dong Wang:** Supervision, Writing – review & editing, Methodology, Resources, Funding acquisition. **Wangcheng Zhang:** Conceptualization, Methodology, Supervision, Writing – review & editing.

Declaration of Competing Interest

The authors declare that they have no known competing financial interests or personal relationships that could have appeared to influence the work reported in this paper.

Data availability

Data will be made available on request.

Acknowledgments

This paper was supported by the National Natural Science Foundation of China (through grant of No. 42025702).

References

Akinci, L., Sawyer, D., 2016. Deriving the rate of salt rise at the Cape Fear slide using new seismic data. In: Submarine Mass Movements and their Consequences. Advances in Natural and Technological Hazards Research, vol. 41. Springer, Cham, pp. 393–400.
Bažant, Z.P., Zi, G., McClung, D., 2003. Size effect law and fracture mechanics of the triggering of dry snow slab avalanches. J. Geophys. Res.-Solid Earth 108 (B2), 2119.
Chen, X., Li, D., Tang, X., Liu, Y., 2021. A three-dimensional large-deformation random finite-element study of landslide runout considering spatially varying soil. Landslides 18 (9), 3149–3162.
Dassault Systèmes, 2014. Abaqus Version 6.14 Documentation. Dassault Systèmes Simulia Corp, Providence, R.I.
Dey, R., Hawlader, B., Phillips, R., Soga, K., 2015. Large deformation finite-element modelling of progressive failure leading to spread in sensitive clay slopes. Géotechnique 65 (8), 657–668.
Dey, R., Hawlader, B., Phillips, R., Soga, K., 2016. Modeling of large-deformation behaviour of marine sensitive clays and its application to submarine slope stability analysis. Can. Geotech. J. 53 (7), 1138–1155.
Duncan, J.M., 1996. State of the art: limit equilibrium and finite-element analysis of slopes. J. Geotech. Eng. 122 (7), 577–596.
Elger, J., Berndt, C., Rüpke, L., Krastel, S., Gross, F., Geissler, W.H., 2018. Submarine slope failures due to pipe structure formation. Nat. Commun. 9 (1), 715.
Garagash, D.I., Germanovich, L.N., 2012. Nucleation and arrest of dynamic slip on a pressurized fault. J. Geophys. Res.-Solid Earth 117 (B10), B10310.
Germanovich, L.N., Kim, S., Puzrin, A.M., 2016. Dynamic growth of slip surfaces in catastrophic landslides. Proc. R. Soc. A. 472, 20150758.
Hill, A., Prakash, A., Hampson, K., Rushton, D., Mackenzie, B., Puzrin, A., 2015. Geotechnical challenges in the Caspian Sea. In: Offshore Technology Conference, Houston, Paper OTC-25988-MS.
Kaya, A., Alemdağ, S., Dağ, S., Gürocak, Z., 2016. Stability assessment of high-steep cut slope debris on a landslide (Gumushane, NE Turkey). Bull. Eng. Geol. Environ. 75 (1), 89–99.
Kovacevic, N., Jardine, R.J., Potts, D.M., Clukey, C.E., Brand, J.R., Spikula, D.R., 2012. A numerical simulation of underwater slope failures generated by salt diapirism combined with active sedimentation. Géotechnique 62, 777–786.
Kvalstad, T.J., Andresen, L., Forsberg, C.F., Berg, K., Bryn, P., Wangen, M., 2005a. The Storegga slide: evaluation of triggering sources and slide mechanics. Mar. Pet. Geol. 22 (1–2), 245–256.
Kvalstad, T.J., Nadim, F., Kaynia, A.M., Mokkelbost, K.H., Bryn, P., 2005b. Soil conditions and slope stability in the Ormen Lange area. Mar. Pet. Geol. 22 (1–2), 299–310.
L'Heureux, J.S., Longva, O., Steiner, A., Hansen, L., Vardy, M.E., Vanneste, M., Haflidason, H., Brendryen, J., Kvalstad, T.J., Forsberg, C.F., Chand, S. Kopf, A., 2012. Identification of weak layers and their role for stability of slopes at Finneidfjord, Northern Norway. In: Submarine Mass Movements and Their consequences. Advances in Natural and Technological Hazards Research, vol. 31. Springer, Dordrecht, pp. 321–330.
Lafuerza, S., Sultan, N., Canals, M., Lastras, G., Cattaneo, A., Frigola, J., Costa, S., Berndt, C., 2012. Failure mechanisms of Ana Slide from geotechnical evidence, Eivissa Channel, Western Mediterranean Sea. Mar. Geol. 307–310, 1–21.
Leynaud, D., Mulder, T., Hanquiez, V., Gonthier, E., Regert, A., 2017. Sediment failure types, preconditions and triggering factors in the Gulf of Cadiz. Landslides 14 (1), 233–248.
Lin, C.H., Kumagai, H., Ando, M., Shin, T.C., 2010. Detection of landslides and submarine slumps using broadband seismic networks. Geophys. Res. Lett. 37 (22), L22309.
Liu, Y., Chen, X., Hu, M., 2022. Three-dimensional large deformation modeling of landslides in spatially variable and strain-softening soils subjected to seismic loads. Can. Geotech. J. 60 (4), 426–437.
Locat, A., Leroueil, S., Bernander, S., Demers, D., Jostad, H.P., Ouehb, L., 2011. Progressive failure in eastern Canadian and Scandinavian sensitive clays. Can. Geotech. J. 48 (11), 1696–1712.
Masson, D.G., Harbitz, C.B., Wynn, R.B., Pedersen, G., Løvholt, F., 2006. Submarine landslides: processes, triggers and hazard prediction. Phil. Trans. R. Soc. A 364, 2009–2039.
Micallef, A., Masson, D.G., Berndt, C., Stow, D.A.V., 2007. Morphology and mechanics of submarine spreading: a case study from the Storegga Slide. J. Geophys. Res.-Earth Surf. 112, F03023.
Palmer, A.C., Rice, J.R., 1973. The growth of slip surface in the progressive failure of over-consolidated clay. Proc. R. Soc. Lond. A 332, 527–548.
Puzrin, A.M., Germanovich, L.N., Kim, S., 2004. Catastrophic failure of submerged slopes in normally consolidated sediments. Géotechnique 54, 631–643.
Puzrin, A.M., Gray, T.E., Hill, A.J., 2015. Significance of the actual nonlinear slope geometry for catastrophic failure in submarine landslides. Proc. R. Soc. A. 471, 20140772.
Quinn, P.E., Diederichs, M.S., Rowe, R.K., Hutchinson, D.J., 2011. A new model for large landslides in sensitive clay using a fracture mechanics approach. Can. Geotech. J. 48 (8), 1151–1162.
Quinn, P.E., Diederichs, M.S., Rowe, R.K., Hutchinson, D.J., 2012. Development of progressive failure in sensitive clay slopes. Can. Geotech. J. 49 (7), 782–795.
Randolph, M., Cassidy, M., Gourvenec, S., Erbrich, C., 2005. Challenges of offshore geotechnical engineering. In: Proceedings of the International Conference on Soil Mechanics and Geotechnical Engineering, vol. 16, p. 123.
Skempton, A.W., 1985. Residual strength of clays in landslides, folded strata and the laboratory. Géotechnique 35 (1), 3–18.
Stoecklin, A., Friedli, B., Puzrin, A.M., 2017. Sedimentation as a control for large submarine landslides: mechanical modeling and analysis of the Santa Barbara basin. J. Geophys. Res.-Solid Earth 122 (11), 8645–8663.
Strasser, M., Stegmann, S., Bussmann, F., Anselmetti, F.S., Kopf, A., 2007. Quantifying subaqueous slope stability during seismic shaking: Lake Lucerne as model for ocean margins. Mar. Geol. 240, 77–97.
Strout, J.M., Tjelta, T.I., 2005. In situ pore pressures: What is their significance and how can they be reliably measured? Mar. Pet. Geol. 22 (1–2), 275–285.
Sultan, N., Cochonat, P., Foucher, J.P., Mienert, J., 2004. Effect of gas hydrates melting on seafloor slope instability. Mar. Geol. 213, 379–401.
Troncone, A., Pugliese, L., Parise, A., Conte, E., 2022. A simple method to reduce mesh dependency in modelling landslides involving brittle soils. Géotech. Lett. 12 (3), 167–173.
Troncone, A., Pugliese, L., Parise, A., Conte, E., 2023. Analysis of a landslide in sensitive clays using the material point method. Geotech. Res. 40 (XXXX), 1–11.

Uenishi, K., Rice, J.R., 2003. Universal nucleation length for slip-weakening rupture instability under nonuniform fault loading. J. Geophys. Res.-Solid Earth 108 (B1), 2042.

Vanneste, M., Sultan, N., Garziglia, S., Forsberg, C.F., L'Heureux, J., 2014. Seafloor instabilities and sediment deformation processes: the need for integrated, multi-disciplinary investigations. Mar. Geol. 352, 183–214.

Viesca, R.C., Rice, J.R., 2012. Nucleation of slip-weakening rupture instability in landslides by localized increase of pore pressure. J. Geophys. Res.-Solid Earth 117, B03104.

Wang, C., Hawlader, B., Perret, D., Soga, K., Chen, J., 2021. Modeling of initial stresses and seepage for large deformation finite-element simulation of sensitive clay landslides. J. Geotech. Geoenviron. 147 (11), 04021111.

Zhang, W., Puzrin, A.M., 2022. How small slip surfaces evolve into large submarine landslides—insight from 3D numerical modelling. J. Geophys. Res.-Earth Surf. 127.

Zhang, W., Wang, D., Randolph, M.F., Puzrin, A.M., 2015. Catastrophic failure in planar landslides with a fully softened weak zone. Géotechnique 65 (9), 755–769.

Zhang, W., Wang, D., Randolph, M.F., Puzrin, A.M., 2016. Dynamic propagation criteria for catastrophic failure in planar landslides. Int. J. Numer. Anal. Methods Geomech. 40 (17), 2312–2338.